UNIVERSITA' DEGLI STUDI DI PADOVA

Scaffolds ceramici da polimero preceramico tramite stampante 3D

Preceramic polymer-derived ceramic scaffolds by 3D-printing

FACOLTA' DI INGEGNERIA

DIPARTIMENTO DI INGEGNERIA INDUSTRIALE

TESI DI LAUREA MAGISTRALE

IN INGEGNERIA DEI MATERIALI

Relatore: *Prof. Paolo Colombo*

Correlatore: *Prof. Enrico Bernardo, Prof. Jens Günster*

Laureando: Omar Sanson

Anno accademico:2013-2014

INDEX

ABSTRACT

Different kind of powders material were studied for the production of ceramic tablets and ceramic scaffolds; the samples were created using 3d printing machine; The aim of this study was to apply the three-dimensional printing (3D-printing) technique to a mixture of a commercial silicone preceramic polymer (MK) embedding micro-sized fillers for the production of bioceramic tablets and scaffolds.

Contrary to a 3D-printing process using a typically sacrificial binder, the approach discussed in this work employs the silicone polymer as a non-sacrificial binder, since the polymer leaves a ceramic residue (SiO_2) with a high yield upon pyrolysis. This ceramic residue moreover can react with the fillers (AP40, a proprietary bio glass-ceramic, and $CaCO_3$) in order to generate the desired assembly of phases, in particular wollastonite and apatite, which are well known bioceramic phases.
Two different compositions have been tested, one with little MK and the other one containing much more MK, namely:

- Solution 1: 20 wt% Wollastonite (after pyrolysis, from the reaction of MK and $CaCO_3$) , and 80 wt% Glass (AP40)
- Solution 2: 60 wt% Wollastonite (MK + $CaCO_3$), and 40 % Glass (AP40)

Two different strategy has been adopted to prepare the two solution:

- Preparation A: MK,AP40 and $CaCO_3$ were dissolved in isopropanol and poured in the water; then the material was separated from the water, milled and sieved;
- Preparation B: MK,AP40 and $CaCO_3$ were dry mixed and isopropanol micro drops were sprayed on the layer of powder; than it was sieved.

Some of the samples produced have been characterized moreover has been analyzed by density measurements, biaxial strength testing, solubility in trisHCl buffer and biology behavior.
At last ceramic scaffolds possessing an ordered porosity have been produced with one of the two selected compositions (solution 1).

CHAP.1: INTRODUCTION

1.1 Motivation

In this thesis, two different powders solutions were printed by powder based three dimensional printing machine. The two different solutions are called solution1 and solution2 and they are mixture of commercial silicone preceramic polymer (MK), filled with AP40 and $CaCO_3$ micro-powder material.
A study on the two powder solution and their printability were performed at BAM (Federal Institute for Materials Research and Testing) in Berlin.
Some XRD and DTA analysis were also carried out at Padua University.
The aim of this research was to analyze the tablets and scaffolds printed with the two solutions.
In the first period preparation A was followed to preparing the two solutions; after the inadequate results achieved by this strategy, a new preparation way, called preparation B, was followed.
In this way, the quality of powder was improved for the two solutions, in particular about the flowability and printability.
It was proved during this research that not only it is possible to print tablets with both solutions, but also, with solution1,to print a scaffold with highly ordered large pore coordination.

1.1.1 3D SCAFFOLD IN RAPID PROTOTYPING

An important requirement for rapid prototyping of medical implants is the possibility to print biocompatible powder.
The demand for biomaterials to repair or replace the bone tissue lost for disease of injury has increase in the last years (1). It is reported that a lot of biomaterials available on the market are ceramics. These include especially calcium sulphate(2), calcium phosphate ceramic and bioactive glasses (3).
Another important class of biomaterial is the Ca-Si-based bioactive glasses that can induce the formation on the surface of Hap layer or hydroxyl carbonated apatite in simulated body fluid.
Furthermore the development of bone tissue engineering methods requires implantable scaffolds with a define shape, size and inter-connective porosity.
The new RP methods introduced the possibility to produce complex geometries, for example 3D scaffolds that were produce during this research by powdered based 3D printing machine.
From the process point of view, one of the main important thing about 3D printing technique is a powder with good flowability and a controlled particle size distribution;

the approach followed in this research was to dissolves the MK powder in order to glue the others two fillers: AP40 and $CaCO_3$. In this way three dimensional object is possible to create and, using pre-ceramic material, after heat treatment a complete ceramic material is obtained.
In the following paragraphs will be explained the different Rapid Prototyping techniques, in particular the powder based three dimensional printing machine employed in this research.
In chapter 3 the materials property and characterization will be explained. The experimental part will follow in the chapter 4, in particular the preparationA and preparationB will be explained , furthermore there will be introduced the meaning of Hausner ratio and his relation with flowability.
In chapter 5 the printing of tablets and scaffold will be revealed. In chapter 6 it will explain some comparison between printed and pressed sample of solution1,and comparison between solution2 and powders mixtures. Chapter 7 spoke about the best powder mixture obtained, the solution1 preparationB. Characterization of the tablets with biaxial flexure test, solubility test and biology test will be explained in chapter 8.

1.2 INTRODUCTION TO ADDITIVE MANUFACTURING PROCESSES

The term Rapid Prototyping (or RP) is used in a variety of processes to describe a process for rapidly creating a system before final release or commercialization. In other words, the emphasis is on creating something quickly and that output is a prototype or basis model from further models and eventually the final product will be derived.
Users of RP technologies have come to realize that this term is inadequate and does not effectively describe the more recent applications of this technology. Improvements in the quality of the output from these machines have meant a much closer link to the final product. Furthermore with rapid prototyping technologies it is possible to produce parts of an object or a whole object which is impossible to create with the "traditional" machining processes, for example: boring, milling, drilling, shaping, turning, broaching etc.
Particularly in these last years many parts are in fact made with additive manufacturing machines; so it is inappropriate to label them as "prototypes".(4)
In the following paragraph a general introduction of the more important Rapid Prototyping technologies will be given and 3D printing will be widely explained.(5)
The most important additive manufacturing processes are:

- Stereolithography (SL)
- Fused deposition modeling (FDM)
- Ink Jet Printing (IJP)
- Three dimensional Printing (3D-P)
- Selective laser sintering (SLS)

- Laminated Object Manufacturing (LOM)
- Direct metal laser sintering

1.2.1 Stereolithography (SL)

This term was coined in 1986 by Charles W.Hull and is one of the most widely used rapid prototyping technologies. It was the first rapid prototyping technologies introduced in 1988 by 3D System,Inc. and it can produce highly accurate and detailed polymeric parts. Briefly and in general terms, these technologies provides the possibility to generate a three-dimensional object by forming cross-sectional laminate of that object at the surface of fluid capable to altering its physical state in response to appropriate stimulation. The physical state of the fluid is altered by an ultraviolet laser and each layer is printed one on top of the other; the laser beam traces a cross section of the part pattern on the surface of the liquid resin and it cures and solidifies the pattern traced on the resin and joins it to the previous layer. (6)(7)
The object is then moved down, in a programmed way, by the thickness of one layer and then the next section were formed in the same way. This process continues until the entire object is formed.

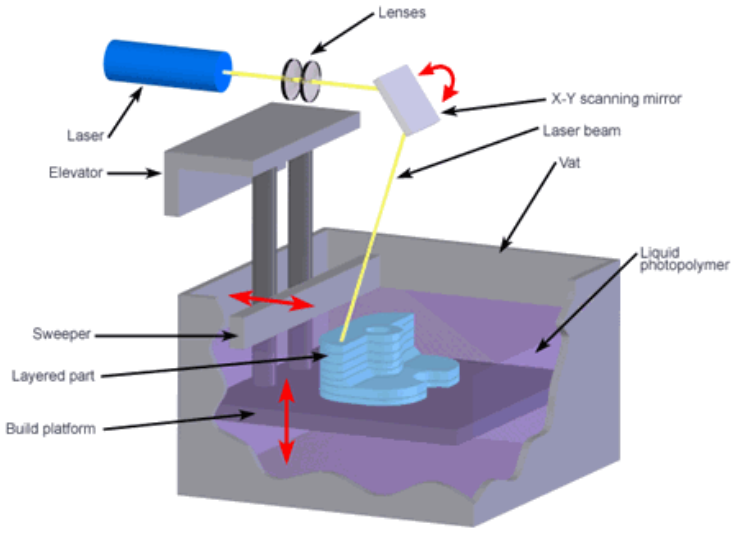

Fig.1 Schematic representation of stereolithography printer

With this technique all kinds of object can be created; complex forms are created by using the function of a computer to help generating the programmed commands.
Using this technologies for example it is possible to print a composite scaffolds with controlled porosity useful in tissue-engineering technique(8). A schematic representation of the process is given in Fig.1.

1.2.2 Fused deposition modeling (FDM)

The technology was developed by S.Scott Crump in the late 1980s and was commercialized in 1990. The term fused deposition modeling and its abbreviation to FDM are trademarked by Stratasys Inc in Minnesota. The exactly equivalent term, fused filament fabrication (FFF) was coined by the members of the RepRap project to give a phrase that would be legally unconstrained in its use.

The FDM method is a RP technique that builds a sample by depositing layer by layer a thermoplastic material. As show in Fig.2 in the FDM method there is an extrusion of molten material through a heated nozzle and a deposition as solid layer on the platform. Once a layer is built, the platform is lowered. The building material is usually supplied in a filament form, but some setups utilize plastic pellets.

The extruder head encloses: the nozzle; a thermocouple for controlling the temperature of material extrusion; a liquefier to melt the material fed through two counter-rotating rollers.

FDM begins with a software process which processes an STL file in minutes, mathematically slicing and orienting the model for the building process; then the head follows a tool-path defined by the CAD file.

A plastic filament wire is unwound from a coil and provides material for the nozzle that is heated to melt the plastic material and can be moved along the X axis and Y axis by a numeric controlled mechanism. The layer thickness and the vertical dimensional accuracy are determined by the extruder die diameter, which ranges from 0,33 to 0,13 mm. In the X-Y plane, 0,025 mm resolution is achievable. A range of materials are available including, polyethylene, polypropylene, ABS etc.

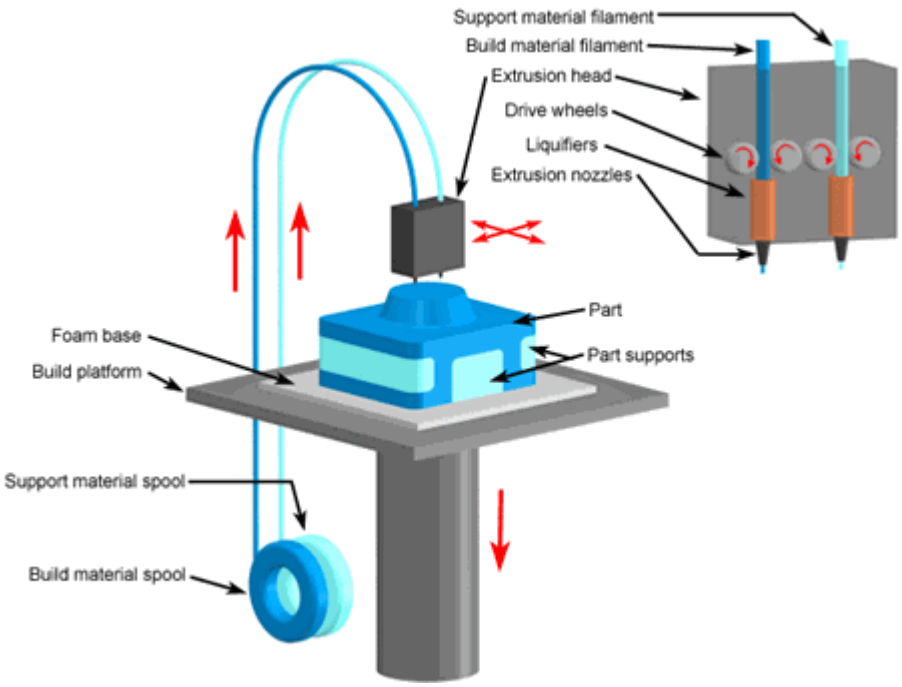

Fig.2 Schematic representation of Fused deposition modeling printer

It is interesting that also with this technology it is possible to build scaffolds for tissue engineered constructs.(9)
In comparison with other free form fabrication methods, FDM does not require any solvent and offers flexibility in material handling and processing.(10)

1.2.3 Ink Jet Printing (IJP)

The Inkjet printing technologies has been implemented by Solidscape Inc. This technology has been used to deposit a very wide range of materials, as ceramics, polymers and metals, for many different applications. Inkjet printing offers the advantages of great accuracy and surface finishes, even though the slow building speed and the fragility of the parts are the most important drawbacks.
As shown in fig.3 the IJP technique is based on the 2D printer technique, but in this case the ink is replaced with thermoplastic materials which is held in a melted state or with liquid medium with appropriate rheological properties containing small solid particles. When printed, liquid drop of these materials immediately cool and solidify to form a layer of the part (11).
Anyway biological materials, including living cells, have been successfully printed.
Regarding the metals printing, there are several kind inkjet printing technique to form metallic deposits. These involve direct printing from a melt, printing a suspension of metallic particles which are then sintered to bind them together, printing a metal compound which is then chemically reduced to form the metal and printing a suitable catalyst followed by electroless plating to deposit the metal.(12)
For ceramics materials there are many different routes which permit to deposit ceramic materials by inkjet printing, which are analogous to some of the methods used for metals.
A suspension of fine ceramics particles can be directly jetted. Several investigators have used sol-gel precursors followed by thermal treatment, for example to deposit barium titanate films and PZT.
As mentioned before also polymeric materials can be deposited by this technologies. Waxes and other relatively short chain polymers with low molecular weights can form readily jettable melts; long chain polymers, however cannot be jetted directly since even as a melt their viscosity is usually too high. The alternative route to deposit these polymers are to dissolve them in a liquid, or create a colloidal dispersion to form a latex, in suitable solvents, although even the presence of high molecular weight of polymer in solution may introduce sufficient viscoelasticity to inhibit good droplet formation.

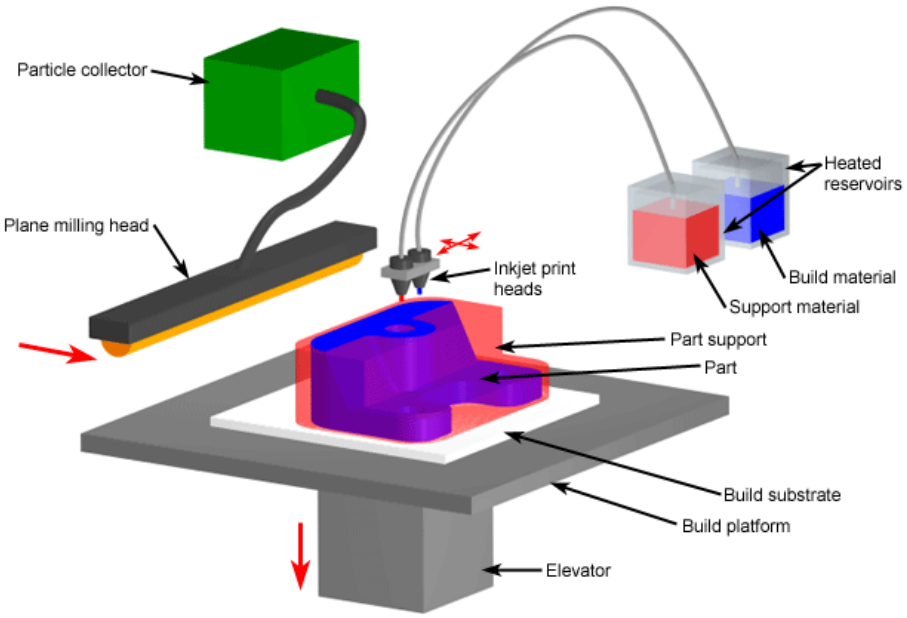

Fig.3 Schematic representation of inkjet printer

1.2.4 Three dimensional Printing (3D-P)

The powder-based three-dimensional printing (3D-P) was developed at the Massachusetts Institute of Technology, USA in 1992 as a method to create preforms from powdered ceramics, metals and polymers. This technology is similar to the Selective Laser Sintering (SLS) process. The 3D-P machines create an individual two dimensional layer by dist ribuiting a layer of powder, by means of a blade or of a roller, on the top of the building chamber. After that a printing head selectively ejects droplets of a binder onto the powder surface and binds the granules in the selected regions. After each layer the platform is lowered according to the thickness of the layer, and new coat of powder is deposited on the last layer. The loose surrounding powder supports the part during building. After finishing the whole process, the unbound powder can be removed with a slight airflow. A schematic representation of one possible setup is presented in Fig.4.

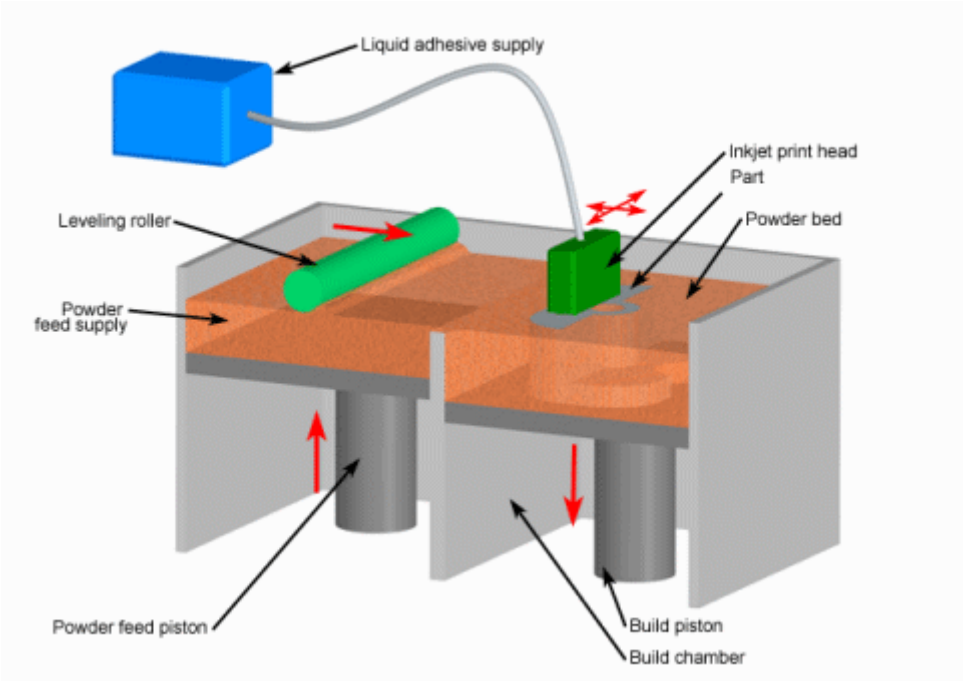

Fig.4 Schematic representation of three dimensional printing machine

This printer offer the possibility to build samples faster than many other additive manufacturing machines, up to 2-4 layers per minute. On the other hand the surface finish and accuracy sometimes are not quite as good as some other additive processes. Anyway by means of this technology it is possible to print a broad variety of materials, including just about anything that is available as a spreadable powder. An extensive literature exists regarding printing of biomaterial parts printed to replace or repair human tissues or damaged organs. (13)

1.2.5 Selective laser sintering (SLS)

Selective laser sintering is an additive manufacturing technique developed and patented by Dr. Carl Deckard and his academic adviser, Dr. Joe Beaman at the University of Texas at Austin in the 1980s. Was Deckard and Beaman were involved in the resulting start-up company DTM, established to design and build the Selective Laser Sintering Machines. As before anticipate this technique is similar to three dimensional printing. Indeed the machine spread a thin layer of powder from the powder feeder to the platform. A laser via scanner controlled by a computer sinters the new powder layer following the pattern of the cross section in the CAD model. Usually the powder is maintained at an elevated temperature so that is fuses easily upon exposure to the laser. The final sample is obtained by removing the unbound powder that serves also as support for the following layers. For ceramic powders, a

post treatment is required to densify the microstructure and to improve the mechanical properties. (14) A schematic representation is show in fig.5.

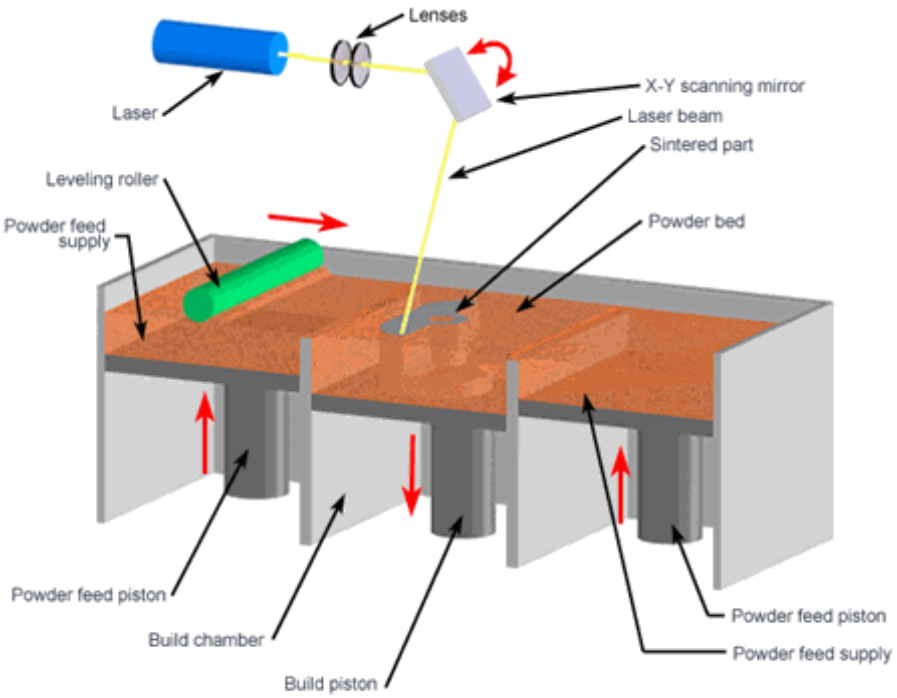

Fig.5 Schematic representation of Selective laser sintering

Recent improvements in accuracy and resolution and reduction of the stair stepping effect have minimized the need for secondary machining and finishing. (15)
It is also interesting the possibility to print metal composite material; in this case SLS process solidify the binder material around steel powder layer by layer, forming the sample.
The object is then placed in furnace at high temperature, the polymer binder is burned off and the part is infiltrated with an alloy which has low melting point to reduce the porosity.

1.2.6 Laminated Object Manufacturing (LOM)

The first commercial laminated object modeling system was shipped in 1991. LOM was developed by Helisys of Torrance, CA. The main components of this printer are: a mechanism that feeds a sheet of the material on a platform, a heated roller that applies a pressure on the layer and a laser LOM builds parts by stacking thin sheets on top of each other, whose contours are according to the part's cross section.(Fig.6)

Some commercial machines supply the sheet material from a roll and use a 50W CO_2 laser to cut the edge; before stacking the sheets, an adhesive is applied over the whole sheets surface.
Another commercial machines uses A3 paper sheets from a standard copy machine that applies the adhesive selectively, only inside the part's contour. After pressing a new sheet onto the previous layer, the sheet is cut with a knife instead of a laser. Originally, all commercial machines used paper foil as material but some years ago, researcher carried out various types of foil made with glass fibers and polymer matrix(16). Those composite materials have high strength, dimensional stability and impact resistance.
Some universities investigated also the use of LOM to fabricate monolithic ceramics parts using SiC and other ceramics; in order to obtain the final ceramic sample, a post process is applied involving pressing, heating and reaction bounding. (17) (18) (19)

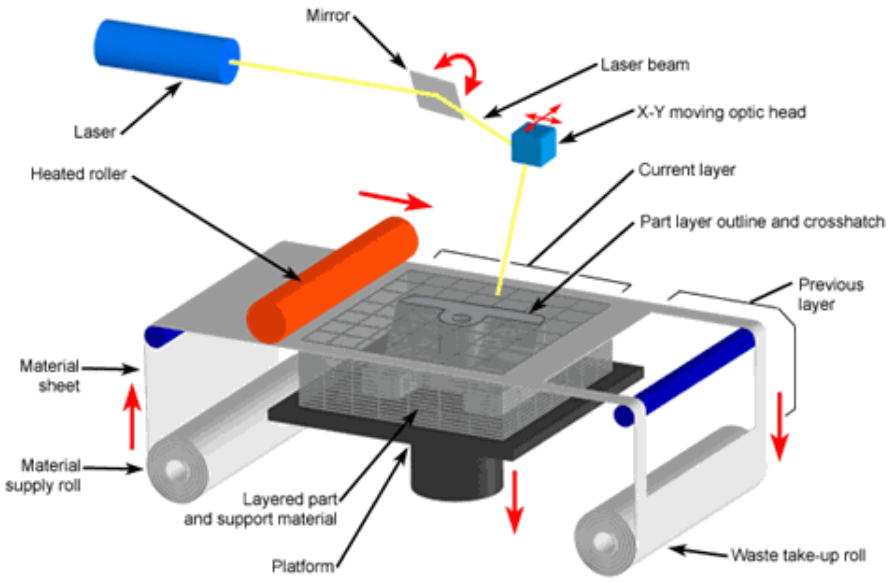

Fig.6 Schematic representation of laminated object modeling

1.2.7 Direct metal laser sintering

This kind of printer was developed by Rapid Product Innovation (RPI) and EOS GmbH in 1994 as the first rapid prototyping method to produce metal samples in a single process. The main part of DMSL is the high laser power beam that melts the metallic powder to build a part with properties similar to the material produced by means of traditional technologies; it is also possible to operate without binders or fluxing agents. Eliminating the polymer binder avoids the burn off and infiltration steps. Compared to SLS, the DMLS permits to build denser parts and moreover the objects have a higher detail resolution due to the use of thinner layers, allowed by the smaller particle dimension of the powder. Nowadays it is possible to use different materials, such as: steel alloys, stainless steel, tool steel, aluminum, bronze, cobalt chrome, and titanium.

In this technique a piston raises the powder supply and then a recoater arm distributes a layer of powder onto the powder bed. Then the powder was sintered by the laser beam. After the deposition of one layer the platform slow according to the thickness of the layer and then the process is repeated.(Fig.7)

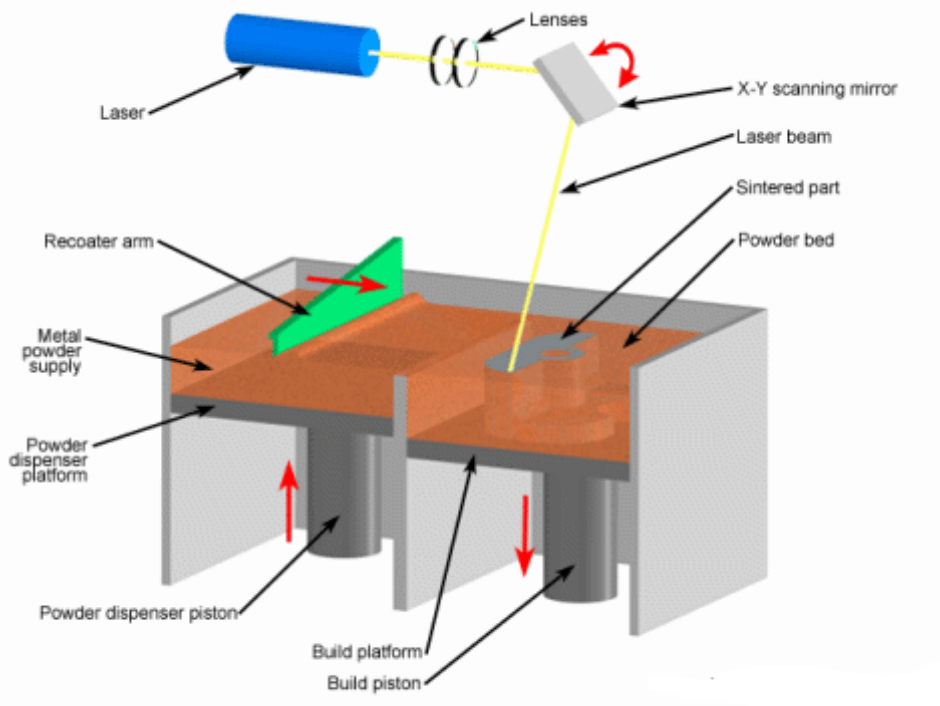

Fig.7 Schematic representation of direct metal laser sintering

1.2.8 Jetted photopolymer

Companies that have developed jetted photopolymer devices include Object Geometries and 3D System.
It is a technique that combines the characteristic of Stereolithography and Inkjet printing. The method to create an object is very similar to an inkjet technique; indeed it uses an array of inkjet print heads to deposit tiny drops of building and support material to form each layer of a part. Often, as in sterolithography, the build material is a liquid acrylate based photopolymer that is cured by a UV lamp after each layer is deposited. The most important advantages of this technique are the surface finish and good accuracy.

1.2.9 Description of the ”powder-based three dimensional printing”

The 3D-printing machine used for this project was a Voxeljet Teststand, VTS 16 (Voxeljet Technology Gmbh, Friedberg, Germany).
The process to build a sample can divided in these important steps:

- A powder feeder deposits the material on the building platform and creates a thin flat layer by means of a blade;
- The printing head ejects tiny drops of solvent to join the particles where the object will be formed;
- The supporting piston lowers the powders bed along the z axis and then the cycle can start again.

Because 3D-printing is a powder-based process where particles are bound, the resulting parts are typically not completely dense, but have a micro-porosity.

It should be noted that every layer thickness was 150 µm, because it was optimized for the spreading of the layers.

Usually a specific software is used to prepare the three dimensional files (often in .STL format) for the 3D-printing machine. This software has a graphical user interface to load the three dimensional file and position it in a virtual building box. The software permits also manipulation of the image, like translation, rotation and automatic positioning. Then the loaded images are sliced to generate the printing matrix of each layer at every z-layer. These images (in bitmap format for the printer used in this work) are loaded in the software that moves the printing head according to the corresponding slice of the file model. When the samples have a simple geometry consisting in a repetition of a limited number of cross-sections, it can be favorable to draw manually the bitmaps of the different slices. Simple freeware graphic tools can be used to do this. This is the case of the tablets and scaffolds produced in this work; an example of the bitmap images used for a tablet geometry is shown in fig.8a, whereas a scaffold can be produced by a sequence of the images shown in fig.8b,8c.

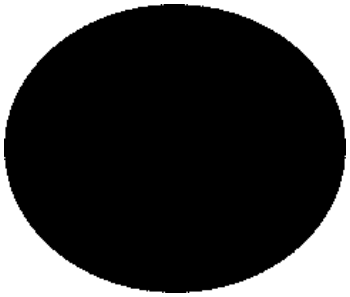

Fig.8a

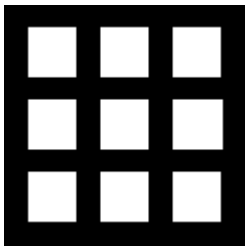

Fig.8b

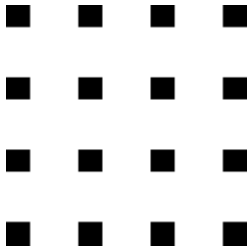

Fig.8c

The Fig.8a represent the bitmap file used for printing a tablet;
The Fig. 8b and 8c represent the bitmap files used for printing the scaffold;

Fig. 9a,9b,9c,9d show the printer machine and main parts of it, in particular fig.9a show the powder based three dimensional printing machine used in this research; fig. 9b show the powder feeder and blade; fig. 9c represented the platform covered by the powder and the printing head and fig.9d revealed the containers installed in the printer and one of these filled with solvent 1-hexanol and hexylacetate.

The printer mounts a printing head with 128 jets (Spectra SL128-AA, Dimatix Fujifilm USA, Santa Clara, CA); in the described experiments a solvent was chosen, which is a mixture of 1-hexanol and hexylacetate (Voxeljet,Ausburg,Germany).
A critical variable for the 3D-printing process is the amount of solvent introduced in the parts. The R parameter of equation (1) is one suitable parameter for expressing this amount. It is a mass ratio of solvent to powder introduced in a part. Since a part is built as a repetition of single voxels (volumetric pixels), and considering that only one drop of solvent is jetted in one voxel, it is possible to express R as the ratio of the mass of drop of solvent to the mass of the powders measured inside a voxel:

$$R = \frac{Drop\ mass}{\rho_{Bulk}(dx \times dy \times dz)} \quad (1)$$

Where $dx \times dy \times dz$ indicated the volume of the voxel and ρ_{Bulk} is the bulk density of the powder. The voxel (volumetric pixel) is volumetric element, representing a value on a regular grid in three dimensional space.
In the setup used in this work, dy was 83 µm determined by geometrical characteristic of the printer and dz, the layer thickness, was 150 µm as determined in a preliminary study to optimize the powder deposition. Therefore the value dx was changed to adjust the R value; dx is connected to the printing head velocity $[v\ (\mu m/s)]$ and to the spitting frequency $[f(Hz)]$:

$$dx = \frac{v}{f} \quad (2)$$

naturally increasing the dimension of the voxel along X axis, the object will be printed with a minor amount of solvent (lower R), since the drop mass remains costant.
It is important to highlight that during the drying stage, some solvent evaporates and the sample becomes stiffer and start to shrinkage slightly. First of all the evaporation start form the surface of the sample.
At this point if too much solvent has been used, the shrinkage can lead to warping the object, indeed the surface exposed to air is compressed more than the lower surface and the liquid is drawn in order to have the same pressure. When the structure is not very permeable, a gradient of pressure is created and the upper surface tends to shrink more than others parts, and the object to warp. Furthermore another problem can occur when a high amount of solvent is introduced during printing: the surplus of solvent spreads and glues the particles close to the object; ; this phenomenon affects the printing resolution and in the worst case it is even impossible print macro-porous scaffold with controlled internal structure.
To ensure a correct control of the solvent in the printed samples, the drop mass was measured before the printing process by measuring the mass of 30000 drops ejected for each of the 128 nozzle and dividing the obtained value by the total amount of drops (30000×128); the measure was repeat three times and averaged.

Fig.9a Powder based three dimensional printing machine used in this research

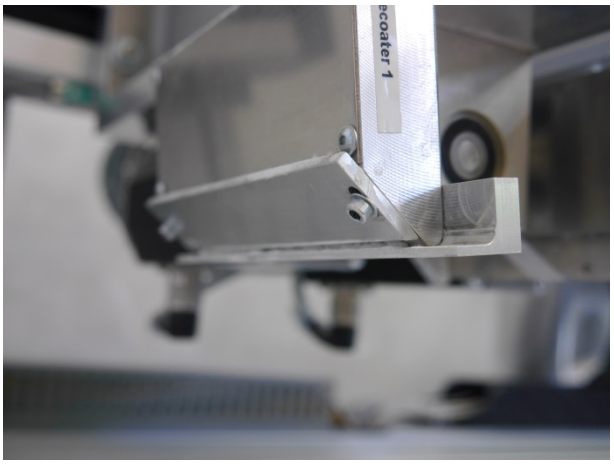

Fig.9b The powder container that deposit the powder and blade that create the layer of powder

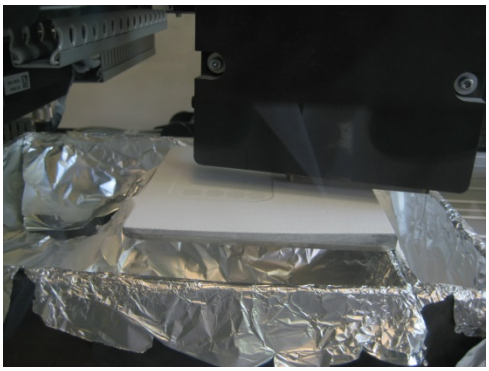

Fig.9c The platform covered by powder and the the head printing

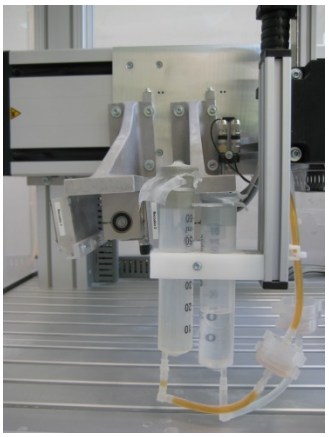

Fig. 9d The contianers installed in the printer filled with solvent 1-hexanol and hexylacetate

CHAP.2: BIOACERAMIC TISSUE

In this chapter follows a presentation of bioceramic materials and different types of bioceramics-tissue interfaces.

2.1 Bioceramic materials

Forty years ago one revolutionary discovery was made about ceramic materials that improved the quality of life of humans. The scientists(20) developed a special design and fabrication of ceramics material for the reconstruction and repair of diseased, damaged or worn out parts of the body. These kinds of materials are called bioceramics. In fact most clinical and surgical applications of bioceramics relate to the repair of skeletal system, composed of bone, joints and teeth, and to augment hard and soft tissue.(21)

Clinical use requires different biomedical properties, such as bioactivity, osteoinduction, osteoconduction, biodegradation and biocompatibility; besides they should be cheap, easily produced, molded and stored.

Bioceramics are made in different form and phases and serve many different functions in the repair of the body. Different phases of the bioceramics can be: singular crystals (e.g. sapphire)(22),polycrystalline (e.g. alumina or hydroxyapatite)(23), glass (e.g. Bioglass)(24), glass-ceramics (e.g. A-W glass-ceramics)(25) or composites (e.g. poly-L-lactide-hydroxyapatite)(26). Surely the properties and functions required determine the choice of the different phases.

For example single crystal sapphire is used as a dental implant because it has high strength, A/W glass-ceramic is usually used to replace vertebrae because it has high strength and bonds to bone, bioactive glasses have low strength but bond rapidly to bone so are used to accelerate the repair of boney defect (27).

Many ceramic compositions are studied for biomedical applications but only few of these have reached human clinical application. Clinical success can be reached with a stable interface and an appropriate mechanical behavior. Few materials satisfy this severe dual requirement for clinical use. (28)

In this last decades a series of calcium phosphate biomaterial has been developed because of his excellent biocompatibility and osteoconductivity(29)(30).

One of the most widely use biomaterial is hydroxyapatite due to its chemical similarity to the inorganic component of hard tissue; anyway in the last years calcium silicate based bioceramics have been studied as potential substitutes, because of their superior bioactivity compare to HA (31). This property is attributed to the presence of silicon, which plays an essential role in the metabolic events that induce a new bone formation; wollastonite is the most common calcium silicate biomaterial proposed for

bone tissue engineering. One important drawback of the calcium silicate bioceramics is their relatively fast dissolution that could comprise their mechanical property.
This problem can potentially be solved by developing multiphase materials, containing phases like wollastonite and phases like apatite.
Kokubo et al. (32) developed A/W glass-ceramics, composed of wollastonite and apatite; this material is mechanically strong and highly bioactive compared to other biomaterials. It has been used in some medical applications, as bone filler or as a bulk material. In this research the idea of Kokubo was followed producing A/W glass ceramic, composed of wollastonite, apatite in glass ceramic.

2.2 Bioactive glasses

The bioactive glasses are a group of surface reactive glass-ceramic materials. They transform their surface by forming a calcium phosphate rich layer when exposed to physiologic fluids. In general bioactive materials have the property to create a strong bond with living tissue, in particular with the bone, when they are implanted. (33)
Some inorganic reactions commonly occur when a bioactive glass is immersed in a physiological environment:
"Ion exchange", in which modifier cations (mostly Na^+) in the glass exchange with hydronium ions in the external solution; "Hydrolysis", in which Si-O-Si bridges are broken; "Condensation of silanols", in which the disrupted glass network changes its morphology to form a gel-like surface layer; "Precipitation", in which an amorphous calcium phosphate layer is deposited on the gel; "Mineralization", in which the calcium phosphate layer gradually transforms into crystalline hydroxyapatite that mimics the mineral phase naturally contained in vertebrate bones.
In general, glass-ceramic materials are polycrystalline and share properties with both ceramics and glasses. This kind of materials has an amorphous phase and one or more crystalline phase; due to this particular characteristic and depending on the amount and type of crystalline phases developed, the material can have interesting properties, for example, zero porosity, biocompatibility, opalescence, low thermal expansion. These properties can be tailored by controlling the glass composition and the different phases.

2.3 Types of bioceramics-tissue interface

The main important point about the biomaterial is which kind of response is elicited in the host tissue. Often the response occurs at the tissue implant interface and depends upon many factors, listed in table 1 (34).

Tissue Side	Implant Side
Type of tissue	Composition of implant
Health of tissue	Phases in implant
Age of tissue	Phase boundaries
Blood circulation in tissue	Surface morphologies
Blood circulation at interface	Surface porosity
Motion at interface	Chemical reaction
Closeness of fit	Closeness of fit
Mechanical load	Mechanical load

Table 1 Factors affecting implant-tissue interfacial response

There are four important responses that are summarized in table 2. An important point is to avoid the toxic response that kills the cells in the surrounding tissues and release chemicals that can migrate within tissue fluid and cause systemic damage to the patient. One important advantage in ceramics implants is their lack of toxicity.

Implants tissue reaction	Consequence
Toxic	Tissue dies
Biologically nearly inert	Tissue forms a non-adherent fibrous capsule around the implant
Bioactive	Tissue forms an interfacial bond with the implant
Dissolution of implant	Tissue replaces implant

Table 2 Consequences of implant-tissue interaction

Formation of a non-adherent fibrous capsule is the most frequent response of tissues to an implant. It is a protective mechanism in order to isolate the implants from the host; metals and polymers produce this type of interfacial response, also some ceramic materials developed this type of interfacial response, but with a very thin fibrous layer.
The third type of interfacial response is when a bond forms across the interface between implants and the tissue. This is called a “bioactive interface”. The interfacial bond mimics the natural interface that is formed when natural tissues repair themselves and also prevents motion between the two materials. An important characteristic of a bioactive interface is that it changes with time, as do natural tissues, which are in a state of dynamic equilibrium.
When the rate of change of a bioactive interface is sufficiently rapid the material “dissolves” or “resorbs” and is replaced by the surrounding tissues. The degradation products must be no toxic and can be easily disposed of without damage to cells.

2.4 Types of bone at bioceramic interface

Most bioceramic implants are in contact with bone. Bone is a living material composed of cells and a blood supply encased in a strong, interwoven composite structure (35). There are three major components of the cellular structure of bone:

- collagen, which is flexible and very tough;
- hydroxycarbonate apatite, bone mineral, which is the reinforcing phase of the composite;
- bone matrix or ground substance, which performs various cellular support functions.

Cancellous bone and cortical bone are the two kinds of bone that have a large interest for the researchers. Cancellous bone is less dense than the cortical bone and it is also called trabecular or spongy bone. It occurs across the ends of the long bones and is like a honeycomb in cross section. As previously said, it has lower density and so it has also lower modulus of elasticity and higher strain to failure than the cortical bone.

One important problem during the healing process is the weakness of the bone interface due to disease or ageing and certainly the decrease in bond area leads to a decrease in strength. The quality of bone can decrease even due to the presence of the implant or the method of fixation. Indeed localized death of cell can occur especially if bone cement is used to provide mechanical attachment of the device. For example the local rise in temperature when the monomer cross-link to form the polymer can kill some local cells.

Another important problem, called stress shielding, can happen when the implant prevents the bone from being properly loaded.

In this case there is a clinical problem because bone must be loaded in tension to remain healthy. Where the applied load is reduced or the bone is in compression, stress shielding weakens bone; this bone unloaded or loaded in compression will undergo a biological change that leads to bone resorption.

This case will result in either a loosening and fracture of the bone or a deterioration of the implant. The presence of wear debris that often occurs in artificial hip and knee joints accelerates the weakening of the stress shielded bone, because the increased cells activity involved in removal and destroy the foreign wear particles.

Very often the combination of stress shielding, wear debris and motion at interface is especially damaging and usually leads to failure.

In the light of this fact many variables must be considered and different cases can be introduced depending on in which part of the body the biomaterial can be introduced.

CHAP.3: MATERIALS PROPERTIES AND PREPARATION

In this Chapter the materials used in the experiments are introduced and a brief description of the preparation of the powder is presented;
The sintering process and the formation of different phases is also explained.
The different materials that were used for the experiments are:
Bioactive silica-phosphate glasses, called AP40 (36,material patented by BAM) ;composition in wt% for AP40:β-Ca_3 ($P0_4$)24.50,SiO_2 44.30,CaO18.60,Na_2O 4.60,K_2O 0.19,MgO 2.82,CaF_2 4.99;
The preceramic polymer used was a commercially available methylsilicone powder (MK, Wacker-Chemie GmbH, Neunchritz, Germany); it has high reactivity and heat resistance and it is soluble in aromatics, esters, ketones and selected paraffins and chlorinated hydrocarbons.
The calcium carbonate powder (Merck, Germany) is a chemical compound with the formula $CaCO_3$.
As mentioned before two solution, at two extreme compositions regarding the amount of MK polymer, have been studied:

- Solution 1: 20 % Wollastonite (MK + $CaCO_3$) , and 80 % Glass (AP40)
- Solution 2: 60 % Wollastonite (MK + $CaCO_3$), and 40 % Glass (AP40)

At the end, the printed green bodies are consolidated at a temperature of 900°C in a high temperature furnace in ambient air. Wollastonite and Hydroxyapatite will be the main crystalline phases developed during the heat treatment.
The pre-ceramic polymer MK is permanently stable up to 300 °C, and can withstand brief exposure to 350 °C. Above 350 °C and as the temperature rises, the methyl silicone resin undergoes oxidative degradation to silica, carbon dioxide and water. Very little smoke is evolved during this thermal degradation and soot-like decomposition products are not formed. The SiO_2 left behind after decomposition chemically react with CaO that derived from degradation of $CaCO_3$ in CaO and CO_2, and create in this way wollastonite phase. At the same range of temperature, the AP40, a glass ceramic material, under heat treatment develop two crystalline phases, called Wollastonite and Apatite leaving a residual glassy phase.

3.1 Pre-ceramic polymer

Pre-ceramic polymers are particular kinds of polymers that after heat treatment convert into a ceramic material;(37) most of them are precursors for the fabrication of mainly Si-based advanced ceramics, generally denoted as polymer-derived ceramics

(PDCs); there are different kind of pre-ceramic materials, for example, polysilazanes, polysiloxanes, polycarbosilanes, polycarbosiloxane. The polymer precursor, with a tailored chemical composition, after a proper thermal treatment (curing and thermolysis processes) under a controlled atmosphere becomes a ceramic material. In this research a commercial polymethylsiloxane was used, which is a pre-ceramic polymer called MK (Wacker-Chemie GmbH, Munchen, Germany), usually available in powder form. MK is a polymethylsiloxane, with the chemical composition shown in Fig.10, besides a 2% mol hydroxyl and ethoxyl groups as functional units.
After thermolysis process, according to the published literature (38), the hydroxyl and ethoxy functional groups undergo cross-linking reaction at high temperature, generating water and ethanol as follows:

$$\text{-Si-OH + HO-Si-} \rightarrow \text{-Si-O-Si-} + H_2O \quad (3)$$

$$\text{-Si-OH + } CH_3CH_2O\text{-Si-} \rightarrow \text{-Si-O-Si-} + CH_3CH_2OH \quad (4)$$

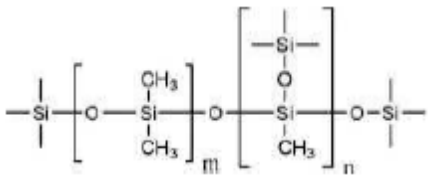

Fig 10 Basic structure of MK polymer

MK in molding compound is permanently stable up to 300 °C, and can withstand for few minutes up to 350 °C; above 350°C and as the temperature rises, the MK undergoes an oxidation degradation to silica, carbon dioxide and water.(39)
At room temperature it is a white powder and the melting rage is between 35-55 °C, and bulk density is 500 Kg/m^3.
This material, like many other pre-ceramic polymers can be shaped or processed using polymer forming techniques, such as injection molding, extrusion, coating from solvent or resin transfer molding etc.. Once formed, this kind of polymer can be converted to a ceramic material by heating it to a temperature high enough to reach the temperature of oxidation.
The conversion occurs with gas release, volume shrinkage and formation of porosity. All these events lead the formation of defects, such as pores and cracks.
The researchers led by Greil (40) showed how a filler mixed with pre-ceramic polymers can serve multiple purposes and have several effects. First of all they serve the purpose of reducing the shrinkage of the component during ceramization and reduce the quantity of defects. Indeed metal particles may react with the gaseous decomposition products, during pyrolysis in inert atmosphere. During conversion of

metal particles into ceramics a volume expansion occurs, limiting the formation of defects and the large shrinkage. Instead inert fillers do not react with the pre-ceramic polymer but simply partially reduce the shrinkage in the component and eliminate the presence of macrodefects (large pores or cracks).
On the other hand the added amount of powder can also constitute the majority of the volume of the sample, and this case the pre-ceramic polymer is used as binder allowing the achievement of higher densities in the final ceramic sample.
The presence of PDC (polymer derived ceramics PDC) can serve the purpose to improve some characteristics, such as corrosion resistance and high temperature creep resistance.
In the experiments described in this thesis, two different kinds of filler were used: AP40 and $CaCO_3$; AP40 was inserted as "passive filler" and $CaCO_3$ as "active filler". Adding different types of filler with the correct amount, it is possible to obtain different phases. For this thesis wollastonite was obtained from MK+$CaCO_3$, and wollastonite, apatite and a glassy phase from AP40 after heat treatment.(41)

3.2 Calcium carbonate

Calcium carbonate is a chemical compound with the formula $CaCO_3$.
Calcium carbonates shared the typical property of the other carbonates; especially important for this research, it releases carbon dioxide upon heating, called thermal decomposition reaction to form calcium oxide:

$$CaCO_3 \rightarrow CaO + CO_2 \quad (5)$$

This decomposition reaction occur above 840 °C in the case of calcium carbonate, in ambient air.

3.3 Wollastonite

Wollastonite is a calcium inosilicate whit chemical composition $CaSiO_3$; usually it can be obtained from the reaction of SiO_2 with different calcium compound, in particular with calcium carbonate:

$$CaCO_3 + SiO_2 \rightarrow CaSiO_3 + CO_2 \quad (6)$$

It the experiments described in this work, wollastonite was developed both from the reaction between MK and $CaCO_3$ (following (6), where the SiO_2 derives from the ceramization of the preceramic polymer and $CaCO_3$ is added as filler in the composition in a stoichiometric amount) and partly form the crystallization of AP40.
MK and calcium carbonate are always mixed with the same mass ratio: MK/ $CaCO_3$=1,4. This ratio was calculated in order to obtain after ceramization the molar

ratio of eq. (6), considering that the MK polymer has a SiO_2 yield of 84wt% after ceramization in air atmosphere.
As it can be seen in the binary diagram SiO_2-CaO in fig.11, at 900 °C the main phase developed is Wollastonite.(42)
Recent studies showed that wollastonite was bioactive and degradable so that might be used as bioactive material in tissue repair or tissue engineering research(43)

3.4 Apatite

Apatite is a group of phosphate minerals, usually referring to hydroxyapatite, fluorapatite, chlorapatite, named for high concentration of OH^-, F^-,Cl^- ions respectively, in the crystal.(44)
The crystal unit cell formulae of the individual minerals are written as $Ca_{10}(PO_4)_6(OH)_2$, $Ca_{10}(PO_4)_6(F)_2$, $Ca_{10}(PO_4)_6(Cl)_2$; for this experiment is used only hydroxyapatite.
In the compositions described in CHAP.3, hydroxyapatite was the secondary phase formed from crystallization of the AP40 glass added as filler.
Hydroxyapatite is one of the frequently used bioceramics for bone and dental tissue reconstitution. It has excellent biocompatibility with hard tissues, and high osteoconductivity and bioactivity despite its low degradation rate.(45)(46)

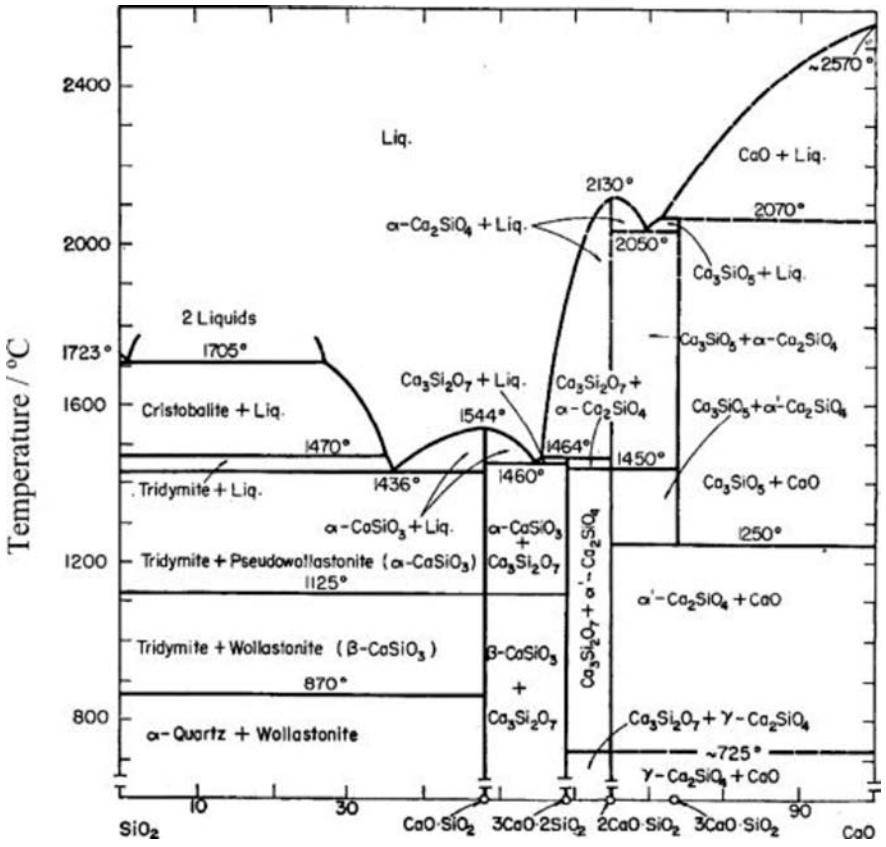

Fig.11 Phase diagram SiO_2 - CaO

3.5 AP40 Analysis and characterization

Fig.12 shows XRD patterns of AP40 powders with different particle size, after crystallization at 900°C for 1h (2°C/min ramp). In tab.3 is indicated the comparison between the XRD intensity of the main peak of wollastonite and apatite in AP40 with different particle sizes, crystallized at 900°C for 1h (2°C/min). It should be pointed out that XRD analysis of glass shows these important points:

- Different particle sizes of the glass powders (<25 µm, 25-45 µm, 45-90 µm,90-100 µm) give very similar XRD pattern.
- The ratio wollastonite/apatite is slightly higher for coarser powders (>45µm) than for finer powders (<45 µm), as shown by the ratio of the XRD main peak for the corresponding phases.
- All spectra indicate the presence of a residual amorphous phase, indeed a wide hump is located at round 32°.

Formulation	Time	Wollastonite	Apatite	W/A ratio
Glass,particle size (<25 µm)	1 hour	425	265	1,60
Glass,particle size (25-45 µm)	1 hour	408	263	1,55
Glass,particle size (45-90 µm)	1 hour	417	239	1,74
Glass,particle size (90-100 µm)	1 hour	505	296	1,71

Table 3_Comparison between the XRD intensity of the main peaks of wollastonite and apatite in AP40 with different particle sizes, crystallized at 900°C for 1h (2°C/min). (These data were collected by Ing. Hamada Elsayed, Padua University)

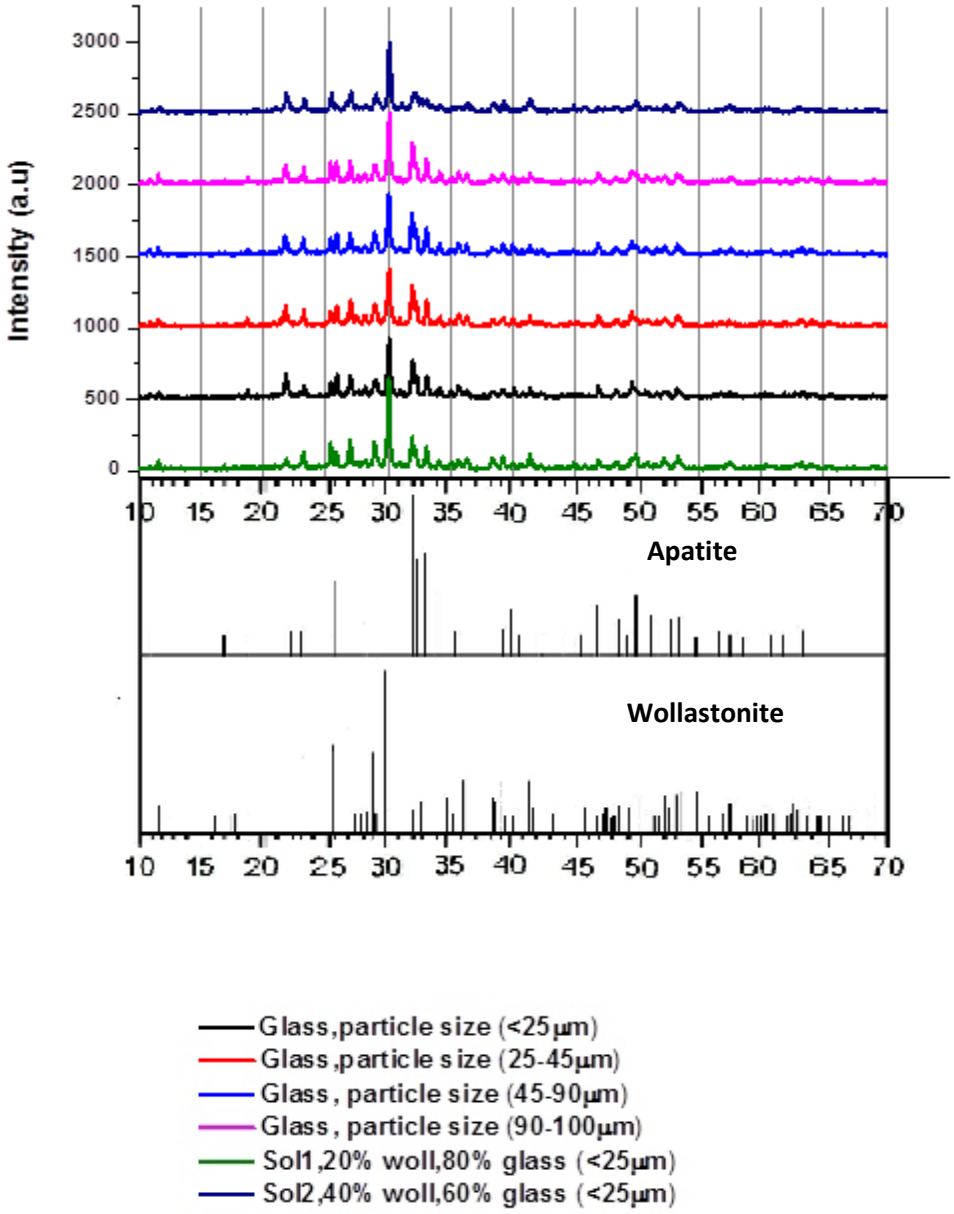

Fig.12 XRD patterns for AP40 with different particle sizes, sol1 and sol2 ;there is not evident trend with the powder size; in agreement with the idea that the crystallization mechanism is a bulk crystallization and not surface crystallization. The main phases developed are wollastonite and hydroxyapatite.
(These data were collected by Ing. Hamada Elsayed, Padua University)

Furthermore the DTA curves for different particle size of the glass powders (<25 µm, 25-45 µm, 45-90 µm,90-100 µm) give the two peaks of crystallization show in Tab.4:

Glass dimension	First crystallization peak	Second crystallization peak
Glass (<25 µm)	775 °C	865 °C
Glass (25-45 µm)	774 °C	879 °C
Glass (45-90 µm)	773 °C	885°C
Glass (90-100 µm)	773 °C	889 °C

Table 4 Represent the dimension of AP40 particles linked with the temperature of the first and second peak of crystallization; the temperatures are very similar.
(These data were collected by Ing. Hamada Elsayed, Padua University)

The first peak corresponds to the crystallization of apatite, while the second corresponds to wollastonite.
It is simple to note how the first and second peak are in the same position, namely at the same temperature, independent of the particles size (Fig.13).
It is known that for smaller particles an increase in specific surface area occurs, so, in the case of a surface crystallization mechanism, the crystallization is expected to start at lower temperatures. Since the DTA peaks positions do not shift when changing the particle size, it can be derived that for the AP40 powder the crystallization mechanism is bulk crystallization and not surface crystallization. This observation is also consistent with the result of the XRD analysis.
.

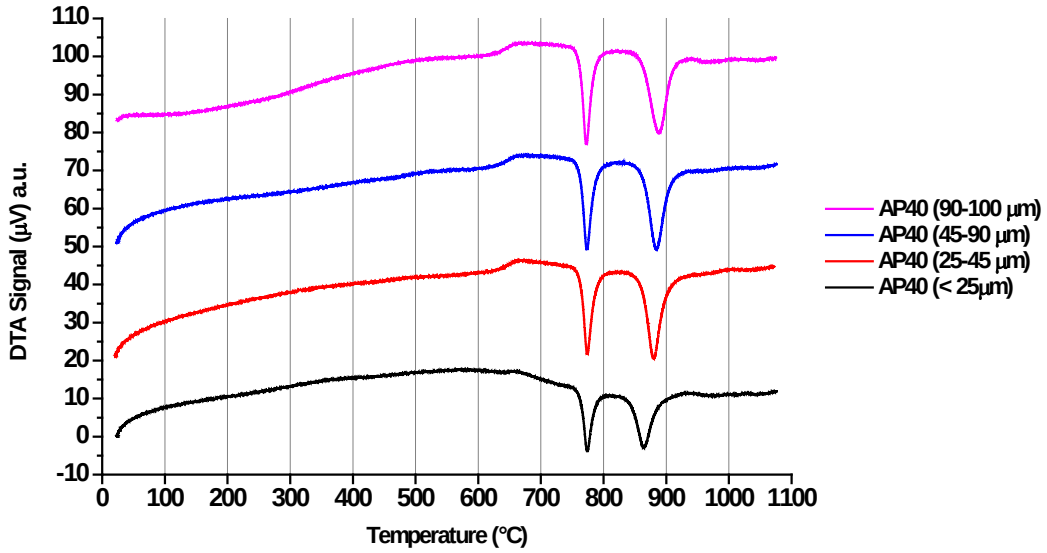

Fig.13 DTA curves of AP40 with the different particles size; the peaks are all in the same position
(These data were collected by Ing. Hamada Elsayed, Padua University)

CHAP.4 PREPARATION AND CHARACTERISATION OF THE POWDER MIXTURE

As described previously, in the experiments hereby described two different kinds of powder mixtures were used, called solution1 and solution2. During this work also two different ways have been developed for the preparation of the powder mixtures, called preparation A and preparation B.

In order to achieve the two aims of both obtaining the expected phases after heat treatment and of producing a 3D-printable powder, the preparation method must generate:

- an effective mixing of the raw materials, in particular of the MK and CaCO3 particles. An inhomogeneous mixing of these two materials may cause the formation of secondary phases other than wollastonite, which is expected to form following eq. (7).

Also, a homogeneous distribution of the MK polymer is important for the 3D-printing process; indeed, in this way the powder should be easier to print since MK, well distributed, when dissolved could glue all other particles.

- a sufficient flowability of the produced powder, which is a very important property for the layer-by-layer deposition in the 3D-printing process.

Solution 1 was designed to obtain 20 wt% of wollastonite from the reaction of MK and $CaCO_3$ and 80 wt% AP40 after heat treatment.

Solution 2 was designed to obtain 60 wt% of wollastonite from the reaction of MK and $CaCO_3$ and 40 wt% AP40 after heat treatment.

It should be noted that the mass ratio MK/$CaCO_3$ =1,4 is constant in the two formulations, as explained in section 2.8.

Briefly, in tab.5 is written the amount of micro-powders that are needed for 10 g of solution1:

MK	$CaCO_3$	AP40
1,20 g	1,70 g	8,00 g

Table 5 Amount of raw materials used to produce 10 gr of powder sol.1.

In tab.6 is written the amount of micro-powders that are needed for 10 g of soution2:

MK	$CaCO_3$	AP40
3,60 g	5,10 g	4,00 g

Table 6 Amount of raw materials used to produce 10 gr of powder sol.2.

Before analyzing the two compositions, it is important to introduce the meaning of flowability for a powder and consequently the Hausner ratio.

4.1 HAUSNER RATIO

The Hausner ratio is a number related to flowability of a powder. The Hausner ratio is calculated by the formula:

$$H = \frac{V_0}{V_f} = \frac{D_f}{D_0} \quad (7)$$

where "V" and "D" represent powder volume and density respectively, subscript "o" denotes the initial or untapped state and "f" the final or tapped state. In the free-flowing powders the initial bulk and tapped densities will be more similar than in poor flowing powders which yield greater differences between the two values.(47)

Indeed the poor flowing powders usually have a large particle size distribution and different particle shape, so the particles can move in the interstices between the particles increasing in this way the tapped density(48)

The important characteristic is tapped bulk density, or simply tapped density: that is, the maximum packing density of the powder achieved under the influence of well-defined, externally applied forces. The minimum packed volume depends on a number of factors including particle size distribution, true density, particle shape and cohesiveness due to surface forces including moisture. Therefore, the tap density of a material can be used to predict both its flow properties and its compressibility.

Hausner ratio standard value is shown in Table 7.(49)

Hausner ratio value	
< 1,11	Excellent flow
1,12-1,18	Good
1,19-1,25	Fair
1,26-1,34	Passable
1,35-1,45	Poor
1,46-1,59	Very poor
>1,60	No flow

Table 7 Represent the value of Hausner ratio

It should be noted that these values are not strictly exact for the powder mixtures measured in this work, because the values were originally obtained for different types of powders. On the other hand, the ranges shown in Table 7 give a qualitative indication of the flowing behavior that in our experience was well corresponding to the ability of the powders to flow and recoat defect-free layers during the 3D-printing process.

4.2 Preparation A

The method can be described like this:

- The pre-ceramic MK was dissolved in 15 ml of isopropanol;
- MK and isopropanol directly mixed with AP40 and $CaCO_3$ for 10 minutes;
- The solution was poured in a baker containing stirred water; in few seconds the solution precipitates;
- The slurry was separated from the water and warmed for 10 hours at 30°C in order to dry the solution;
- The powder was sieved under 100µm

It should be pointed out that the goal in this case is to have a powder with an adequate flowability and well mixed.
The raw materials were sieved before mixing, according to tab. 8

MK	$CaCO_3$	AP40
<45 µm	<10 µm	45-90 µm

Table 8 Dimensions of the particles used for preparationA

The solution 1 and 2 were prepared with the same technique following the amounts written in tab4.
In particular, in a preliminary study for solution 1, three different ways to pour the slurry in the water have been tested:

α)Pour directly in the water during vigorous stirring at room temperature;
β) With a pipette, put the drop of slurry in the water at room temperature;
γ) Warm the water at 70°C and pour directly the slurry.

At the end, all these techniques did not change the quality of the powders and gave powders with similar flowability.
Following the "preparation A" route, the two solutions had these values of flowability:
The Hausner ratio for solution1 : 1,36 = poor
The Hausner ratio for solution2 : 1,39 = poor
In both cases the flowablity was poor and accordingly it was more difficult spread layers of powders on the platform the 3d-printing machine.
The composition of the powders did not seem to have a strong influence on the flowability, whereas this seems to be more determined by the technique used to prepare the mixtures.
Fig.14 shows the particle size distribution for solution 1 α,1 β,1γ and solution2 measured by laser granulometry.

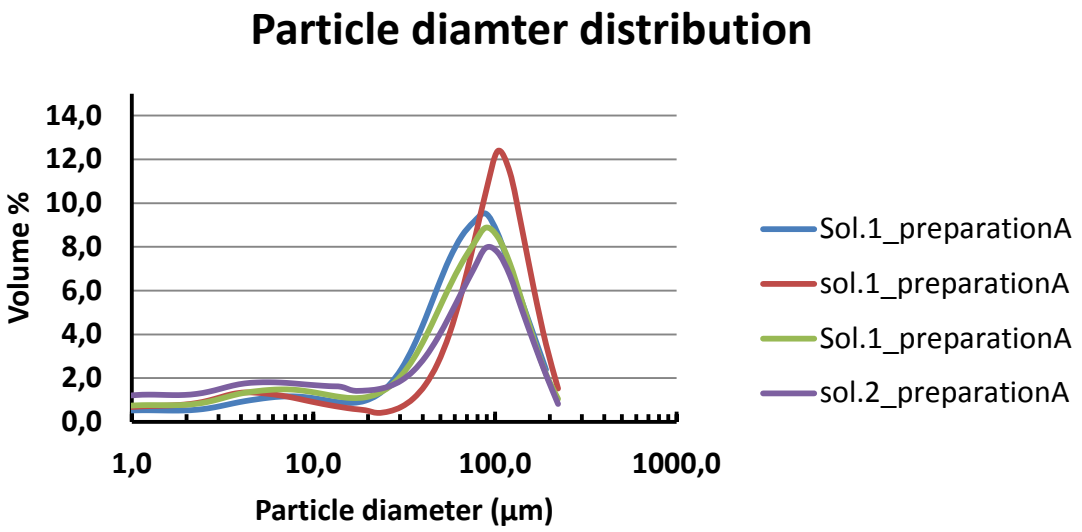

Fig.14 Particle diameter distribution of the particles of sol1 and sol2 preparationA

The result in Fig.14 shows that most of the particles have dimensions between 50 µm and 200 µm. Despite the powders being sieved < 100 µm, a consistent fraction of the powders has a size between 100 µm and 150-200 µm. This might be due to the presence of agglomerates or to a non-perfectly effective sieving. Furthermore the graph show that a consistent fraction of the powders has very small dimension, under 50 µm; certainly, as said previously in the paragraph 3.1, this worsens the flowability of the powders. A possibility would be to sieve the powder fraction with the unwanted small dimension, under 45 µm, but by following this route there would be a possible risk of eliminating some material selectively, thus changing the correct ratio of different powders.

4.3 Preparation B

In the light of this poor result another technique of preparation of the two solutions was used.
The new method can be described like this:

- The three different raw materials were dry mixed with small alumina spheres (a third of volume of the powders)
- No solvent was added;
- The powders and spheres were stirred for 12 hours in turbula machine with the aim of achieving an homogeneous mixing of powdery substance with different specific weight and particle size;
- The powder was separated from the alumina spheres;
- The powder was spread on a plan;

- With air spray gun some tiny drops of isopropanol were sprayed on the powders;
- The drops of isopropanol dissolved the MK particles forming small agglomerate of MK,AP40 and $CaCO_3$;
- The powder was sieved separating the fraction between 45-90 µm from the rest;
- For the rest of the powder the spraying process was repeated until all the powder has the desired dimension.

The solution 2 were prepared with the same technique following the amount written in tab4.
The dimension of the powder show in tab.9

MK	$CaCO_3$	AP40
<45 µm	*c.a 10 µm*	*<45 µm*

Table 9 Dimensions of the particles used for preparationB

With this preparation the two solution have these values of flowability:
The Hausner ratio for solution1 : 1,28 = passable
The Hausner ratio for solution2 : 1,23 = fair
In both cases the flowability improved compared to the preparation method A. Accordingly, these powders were easier spread the powder on the platform. It is important to note that some drawbacks for this kind of preparation exist:

- A lot of time is spent for the sieving process and furthermore only a small fraction of powder have the wanted dimension;
- The process should be repeated several times and in this way some powder can be lost during every cycle (for example: during the spreading of the powder on a plan or during the sieving process).

4.4 Characterization of the powder mixture

In this paragraph is shown the characterization of the powders by scanning electron microscope (SEM) with Energy-dispersive X-ray spectroscope (EDX spectrum)

4.4.1 SEM and EDX characterization

The Fig.15a,15b,15c show SEM pictures of powder solution 1,preparation A:

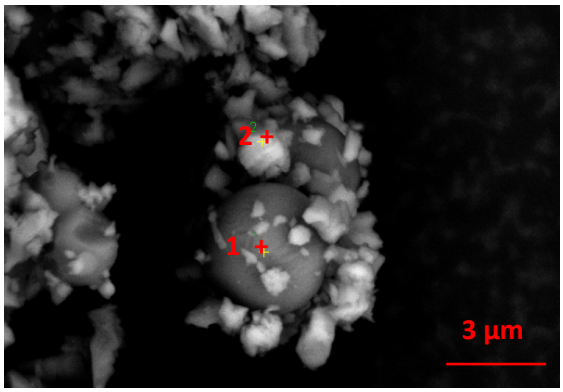

Fig.15a SEM picture of powder solution1 preparationA

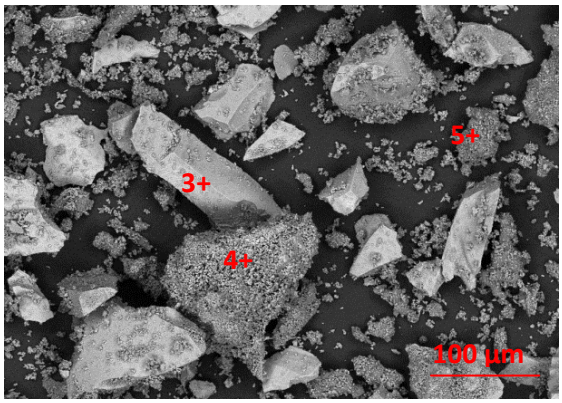

Fig.15b SEM picture of solution1preparationA; the small particles of $CaCO_3$ glued to MK particles.

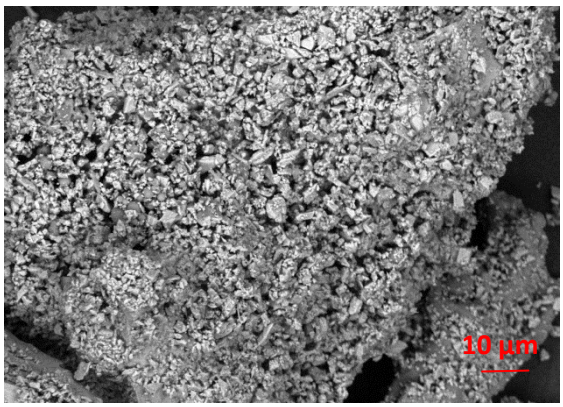

Fig.15c SEM picture of $CaCO_3$ attached at one particle of AP40 in solution1preparationA

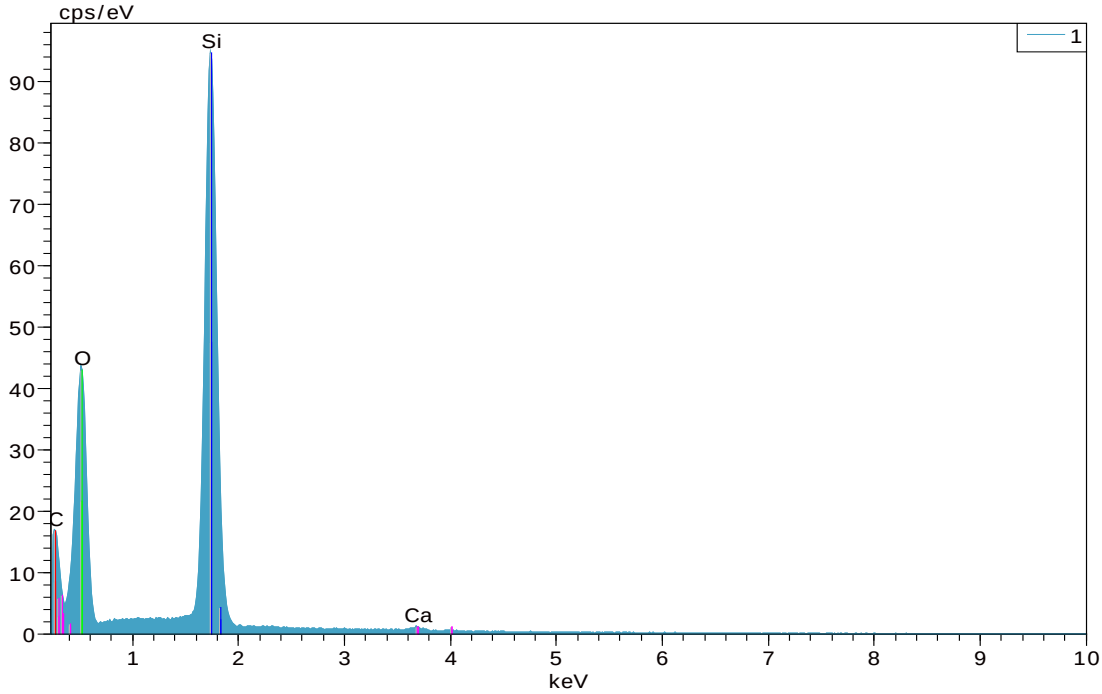

Fig.15d EDX spectrum of point1 in Fig 15a;there are one peak of Si and O revealing the presence of MK

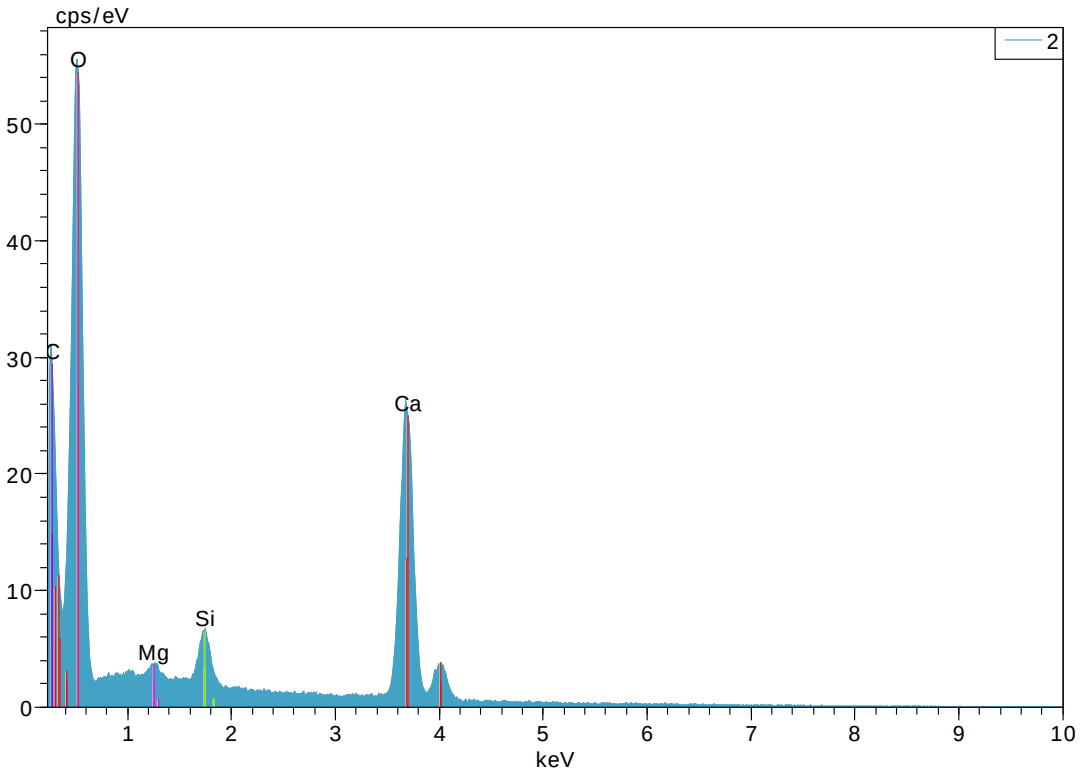

Fig.15e EDX spectrum of point2 in fig 15a; the high peaks of O and Ca revealed the presence of $CaCO_3$

Fig.15b shows an overview of the powder, revealing the distribution of the raw materials. In Fig.15a (point1) the spherical particle is MK; indeed in the EDX spectrum of fig. 15d there is a high peak of Si that as already said before is the main chemical element of MK. It was expected to obtain spherical MK particles due to the processing conditions: when poured in water, the MK polymer precipitates and due to its hydrophobic surface it tends to form a geometry with a minimum surface, which is in this case a sphere.

The small white particles (point2), attached to the MK sphere, are calcium carbonate particles; indeed the EDX in fig.15e shows mainly the peaks of O and Ca.

In some parts there are also MK particles completely covered with calcium carbonate (point 5).

Lastly in fig. 15b the big white particles are AP40 (point n.3), and in some of these there are calcium carbonate particles stuck on the surface (point n.4). The large particles shown are AP40, which was sieved 45-90 µm before mixing. These particles have a typically irregular geometry deriving from the grinding process.

It is interesting to see that there is still an amount of unbound small $CaCO_3$ particles. This is probably the reason for the measured poor flowability of the powder. The presence of spherical MK particles and of rather coarse AP40 was expected to facilitate the powder flow, but it might be that the amount of fine unbound $CaCO_3$ particles was sufficient to hinder the powder flow.

The Fig.16a,16b,16c reveal the powder of solution2.

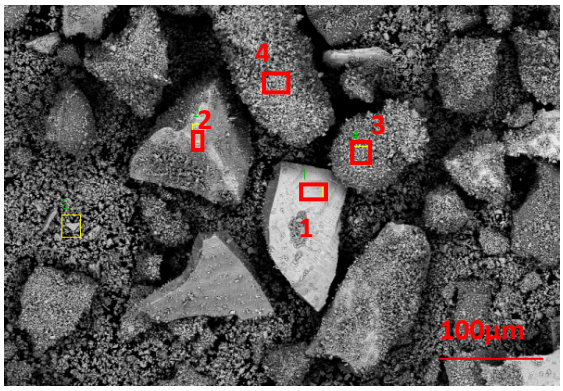

Fig.16a SEM picture of powder solution2preparationA

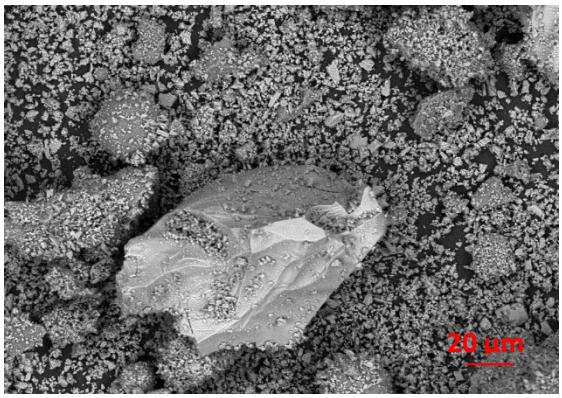

Fig.16b SEM picture,in the center the bigger particle is AP40;then there are some particles of MK;both are surronded by the small partiles of $CaCO_3$

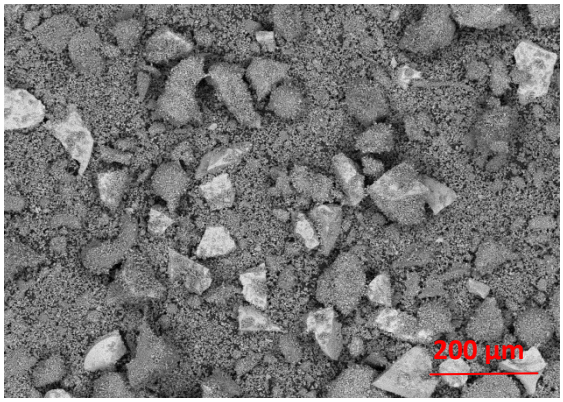

Fig 16c SEM pictures of solution2 preparationA; it is evident that most of the fine $CaCO_3$ particles are unglued

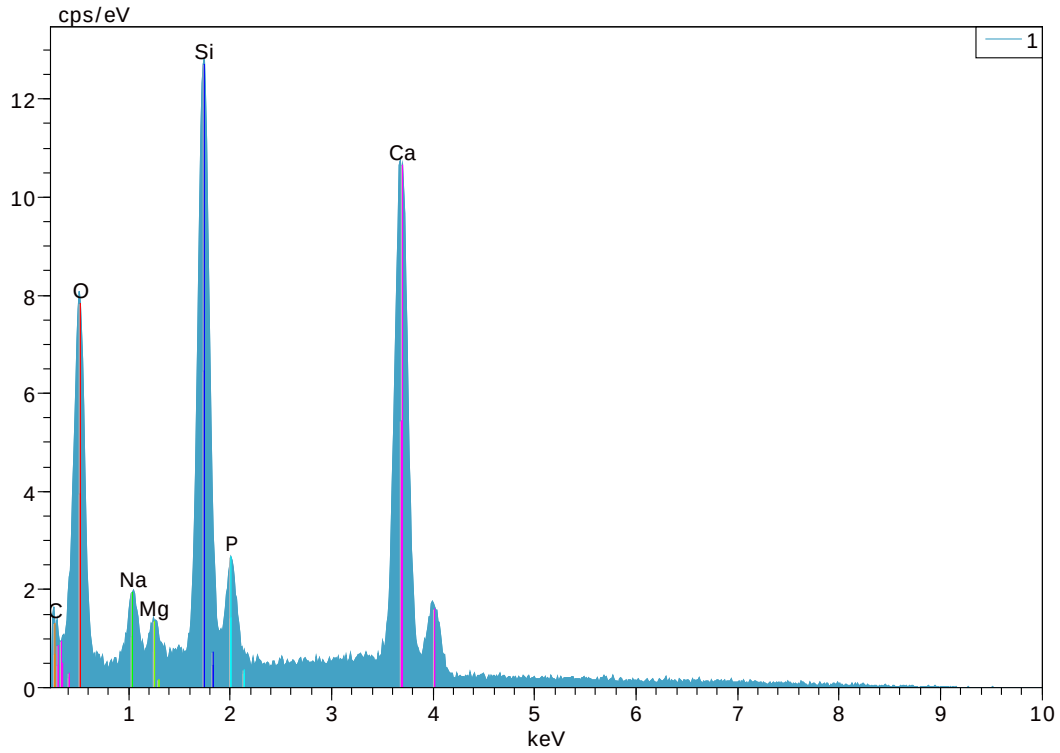

Fig. 16d EDX spectrum of point 1 in fig 16a, show a large amount of Si and Ca suggesting the presence of AP40

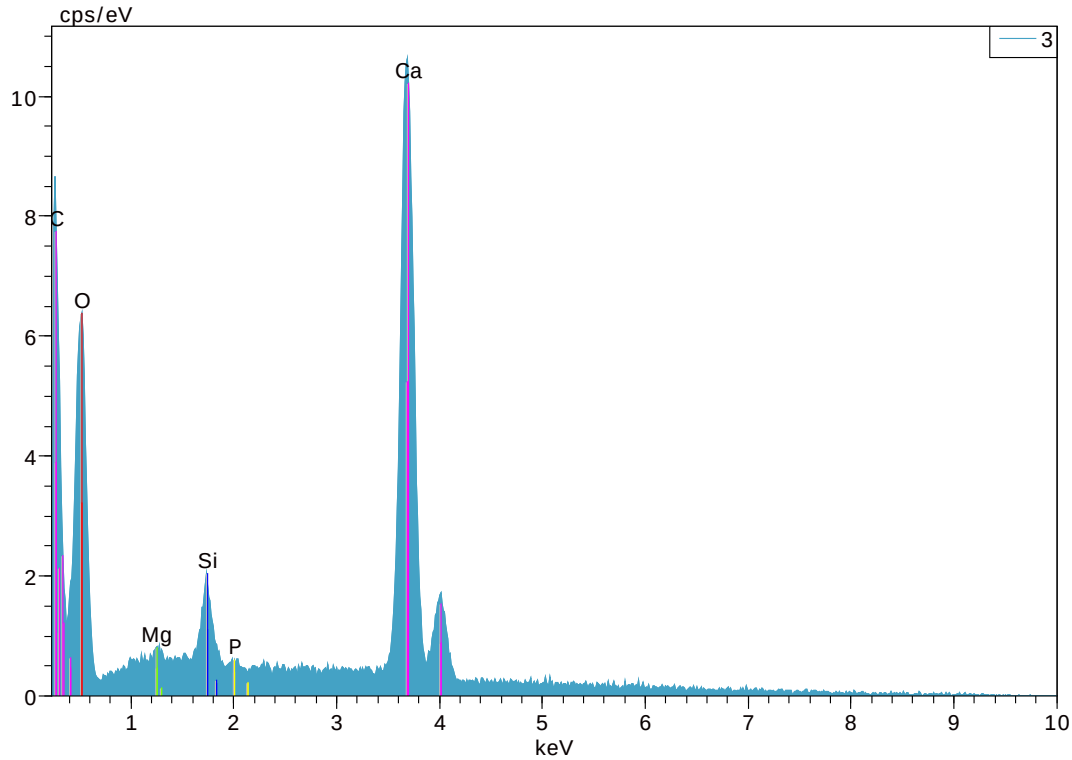

Fig 16e The EDX spectrum of point2in fig.16a reveal two high peaks of Ca and O revealing $CaCO_3$ with AP40 because there also small peak of Si and P.

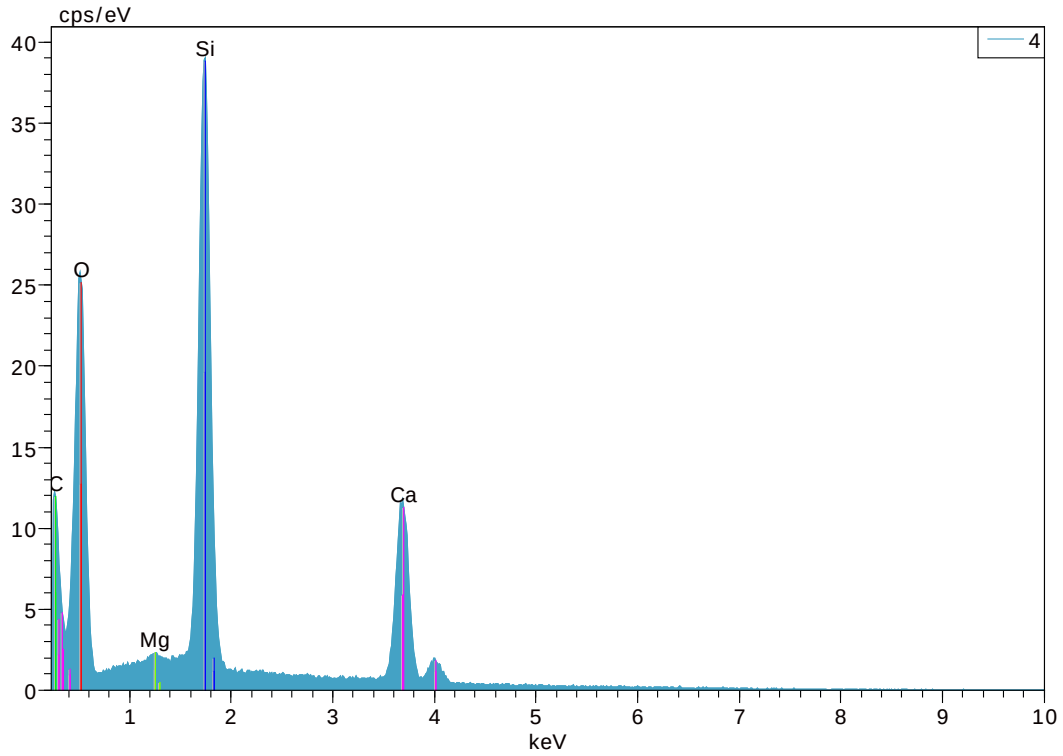

Fig.16f The EDX spectrum of point 3in fig.16a reveal peaks of Si,O and Ca, suggesting that should suggest the presence of $CaCO_3$ glued at MK

Fig.16c shows an overview of the powder mixture. The composition is similar to what observed for solution1, but a larger amount of fine MK and $CaCO_3$ particles are present, compared to the coarse AP40 particles.

The EDX in fig.16d (point1 in figure 16a) shows a large quantity of Si and Ca, together with Mg, Na and P: this particle is surely AP40.

AP40 particles sometimes have a clear surface (point 1), but in other cases they are covered by $CaCO_3$ (point 2 and 4). The EDX spectrum for point 2 is shown in fig. 16e, showing a large amount of Ca and O, but also Si, P and Mg, which can be interpreted as AP40 covered with $CaCO_3$.

Fig.16f shows the EDX relative to point 3 in fig.16a: a large amount of Si, O, Ca can be interpreted as an MK sphere with $CaCO_3$ particles stuck on the surface.

Compared to solution1, solution2 has a larger amount of $CaCO_3$ that worsens the flowing behavior of powder. That is understandable, because as already anticipated the dimension of $CaCO_3$ is c.a. 10 µm, and generally fine powders hinder the flow.

CHAP.5 PRINTING OF TABLETS AND SCAFFOLDS

In this chapter the different attempts to print the tablets are been presented.
The tablets were printed with sol1 preparation A and sol2 preparation A e B; in particular the scaffolds could be printed only with sol1 preparation B.
The shrinkage of the samples after heat treatment is reported and the tablets were characterized by means of porosity and the density measurements. A tablet printed with sol1 preparationA was also characterized by micro-CT.and with a EMI hot stage microscope in order to determine the sintering temperature.

5.1 Characterization tablets sol1 preparationA

Different printing attempts have been made with the purpose of creating precisely printed samples, namely samples with the correct amount of solvent. With this idea in mind, four tablets were printed with four increasing amounts of solvent. To do this, four different Δx values were considered. Δx, as introduced in paragraph (1.2.9), is related to the ratio R, which expresses the solvent concentration in the parts.
Tab.10 shows the dimension of the voxel, the mass of the drop and the mass of the powder in one voxel for the four printed samples. From these values, the R value can be calculated using eq.(1).
As anticipate before R is the most important parameter; with small R values the samples have round corners and are easily damaged after printing while removing the unbound powder with the brush. So, in some case it is impossible reproduce perfectly the tablet. On the other hand more solvent introduces other problems:

- shape distortion when the solvent evaporates
- the excess solvent can spread and glue also others particles. In this way the shape of the part is not respected or it is poorly reproduced.

	Sample1	Sample2	Sample3	Sample4
R	0,042	0,053	0,075	0,106
Drop mass solvent (ng)	57,2	57,2	57,2	57,2
Powder mass (ng)	1347,7	1078,2	754,7	539,1
Delta x (µm)	125	100	70	50
Delta y (µm)	83	83	83	83
Delta z (µm)	150	150	150	150

Table 10 Parameters of printer for tablet solution1

The Fig. 17a,17b,17c show the tablets sol1.

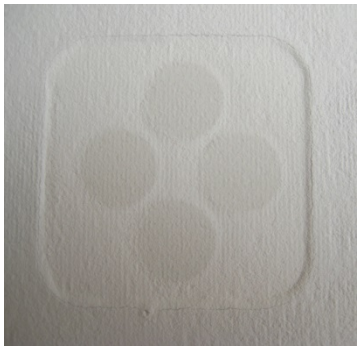

Fig.17a

Fig.17b

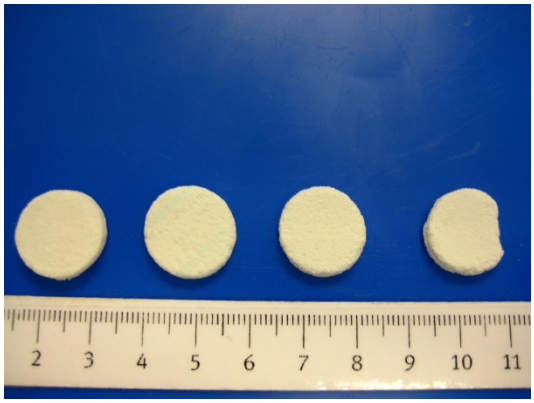

Fig.17a Platform of the printer covered of powder;it is possible to see the four tablet printed;

Fig.17b The platform of the printer showed like in fig.19a, in this case the unbound powder has been removed;

Fig.17c The four tablet of solution1preparationA printed with different R ratio; the solvent concentration used for printing decreases from left to right.

The tablets printed were strong enough to be handled quite easily; in some case a slight shrinkage of the wetted powders materials was observed that affected the geometry of the printed parts. Furthermore the concentration of the printing liquid put in a layer is a very important parameter to consider. It can be noted that when a high level of solvent is introduced, the tablets tends to warp due to stresses introduced by the gradient in solvent concentration, because the evaporation rate is higher in the surface layer and close to it than from the bottom. Sample 3 was geometrically the most precise, therefore other tablets with the same dimension and the same amount of solvent were printed for biaxial strength testing and for solubility test.

The printed tablets were heat treated at 900°C for 1h (2°C/min ramp).

In this context it is noteworthy to report the shrinkage of the tablets after ceramization.

The tab. 11 shows the average sample dimensions and the shrinkage

	Average value	Deviation standard
Diam. Green tablet (mm)	17,23	0,22
thickness green tablet (mm)	3,43	0,12
Weight green tablet (g)	0,76	0,05
Diam. ceramized tablet (mm)	16,41	0,20
Thickness ceramized tablet (mm)	3,35	0,13
Weight ceramized tablet (g)	0,69	0,06
Shrinkage diam.	5 %	0,01
Shrinkage thickness	5 %	0,02

Table 11 Average value of tablets printed with solution1 before and after heat treatment,900°C for 1hour,heating rate 2°C/min, uncontrolled cooling

Fig.20 shows the 3D image of a sample in the ceramic state made by a micro CT technique. The measurement was performed on a Scanco Medical device (µCT40) with a resolution of 12 µm.

Fig.18 3D image of a sample solution1preparatioA by micro-CT technique

This technique permits to evaluate:

- the total porosity;
- the pore size distribution, fig.19;
- the strut size distribution, fig.20.

The total porosity is 0,58 for sample solution1preparationA measured by a micro CT technique.

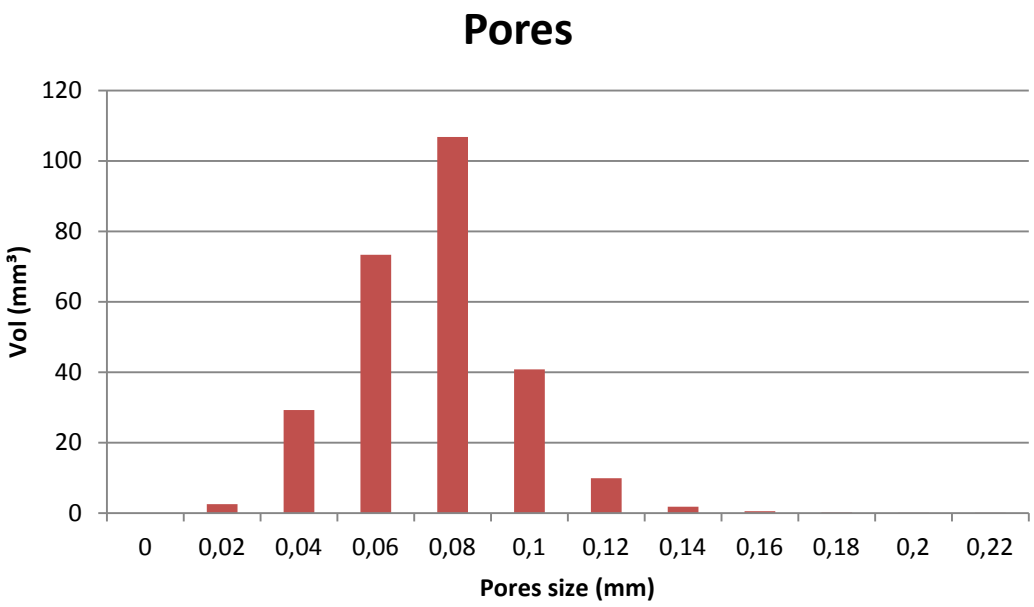

Fig.19 Pore size distribution in a tablet printed with solution1 preparation A. The graph shows that most part of the pores volume is occupied by pores of about 0,08 mm.

The pore size is determined by fitting spheres into the pore volume, where the pore size is considered the diameter of the sphere.

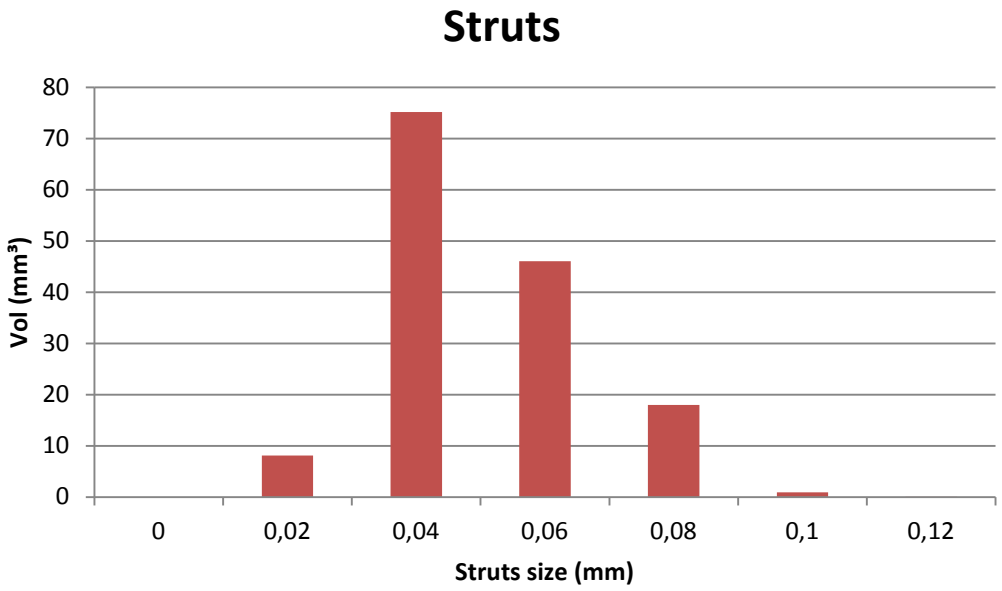

Fig.20 Graphic about dimensions of the struts vs volume occupied by the struts in a tablet printed with solution1preparationA;the graph revealed a large amount of struts with 0,04 mm

Porosity and pores size of biomaterials play a critical role in bone formation in vivo and in vitro (31); it is very important to know the relationship between pores size and porosity of biomaterials in order to know the effect on osteogenisis and the

relationship to the mechanical properties of the scaffold. Fig.19 shows that the sample has several pores between 0,06 mm and 0,10 mm.

A successful scaffold should balance mechanical function with biofactor delivery, providing a sequential transition in which the regenerated tissue assumes function as the scaffold degrades. Depending on the application, it is often considered that it is important to have quite big pores because they allow migration and proliferation of cells.

The minimum pore size required to generate mineralized bone is generally considered to be ~100 µm after the study of Hulbert et al, where a scaffold with 46% were implanted in a dog femorals.(29).Large pores (100-150 µm) showed substantial bone ingrowth, and smaller pores (75-100µm) resulted in ingrowth of unmineralized osteoid tissue. Smaller pores (10-75µm) were penetrated by fibrous tissue.

However another group of researcher have tested a scaffold with four different pore sizes (50,75,100,125 µm) in rabbit femoral defects under non-load-bearing conditions (30). Bone ingrowth was similar in all the pore sizes suggesting that 100µm may not be the critical pore size for non-load-bearing condition.

The bulk density and porosity of the samples were measured using Archimedes technique measuring the dry, saturated and suspended mass in water of 12 samples. The results are reported in tab 12,all the values are indicated with standard deviation:

Apparent density (g/cm^3)	Geometrical density (g/cm^3)	True density (g/cm^3)	Open porosity	Total porosity
1,07 ± 0,06	0,97 ± 0,06	2,77	0,61 ± 0,02	0,61 ± 0,02

Table 12 Value about density and porosity revealed by Archimedian tecnique

Where apparent density is defined as the mass of the dry sample divided by the total volume including the total porosity and defects; geometrical density is defined as the mass of dry sample divided by total volume calculated with the caliper; true density is defined as density of material without pores, measured using pycnometer; open porosity is defined as the volume of open pores divided by the total volume; total porosity is defined by formula (8):

$$Total\ Porosity = (1 - \frac{Apparent\ Porosity}{True\ Density}) \times 100 \quad (8)$$

It is important to note that in this case there is a slight inaccuracy about the value of total porosity.

5.1.1 EMI hot stage microscope

A small cylinder printed with solution1 (preparation A) was also analyzed by EMI hot stage microscope to determine the sintering temperature.

This sample was already heat treated at 900°C, so no variation is expected at least until this temperature. The aim of this study was to determine a possible heat treatment to

further densify the printed parts. The printed samples ceramized at 900°C are still very porous, so for some applications it would be interesting to achieve a further densification in order to increase the mechanical properties. The results here exposed will be employed in a future research work in this direction.

In fig.21 are plotted the variations of geometrical parameters of the cylindrical sample when heated. Fig. 22 also presents selected pictures of the sample at increasing temperatures. This is the ramp used during EMI hot stage microscope analysis: 10°C/min until 900 °C and then 5°C/min until 1400 °C.

One main point is recognized:

- The sintering temperature is a range of temperature starting at about 1100°C. In this range the volume decreases: in this case the instrument measures the area decrease, which is about 20% between 1100°C and 1200°C. The shape of the sample remains the same, which means that no distortion happens in the sample in this interval. The shape factor is defined as the ratio width/height of the sample, and remains constant.

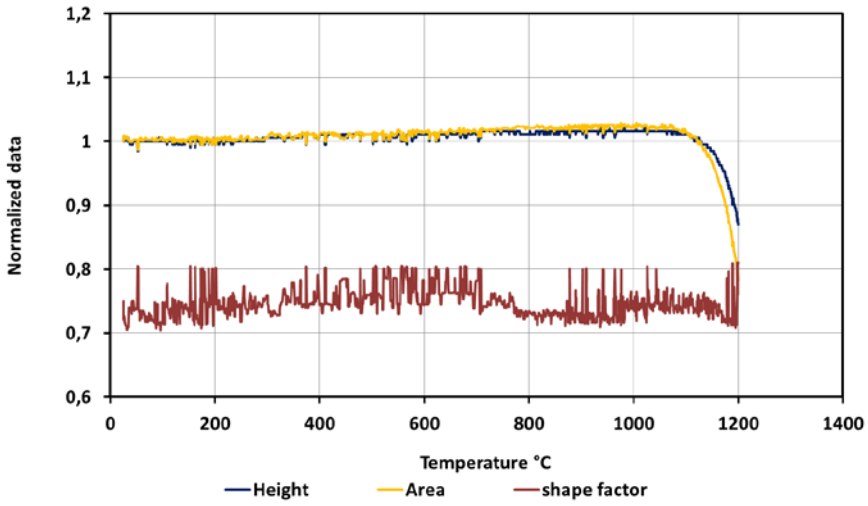

Fig.21 Variation of geometrical parameters with temperature recorded by hot stage microscope. The sample was a cylinder printed with solution1

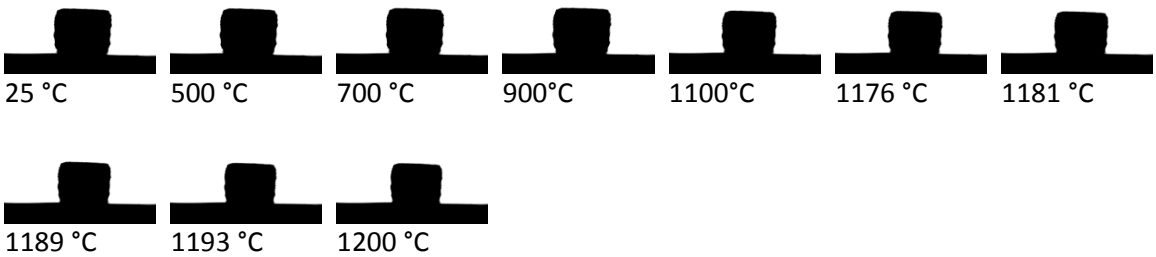

Fig.22 Pictures of sample solution1 under the heating microscope

The fig.23a,23b, show the tablet printed with solution 1 preparation A before and after ceramization. The fig.23c revealed the microscope picture of surface of tablet

sol1preparationA photos show how the solution1 gives samples with a good quality and with a well-defined shape.

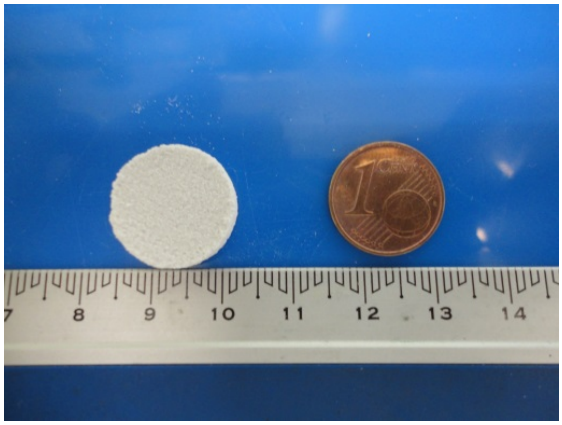

Fig.23a Tablet solution1,preapartionA before heat treatment

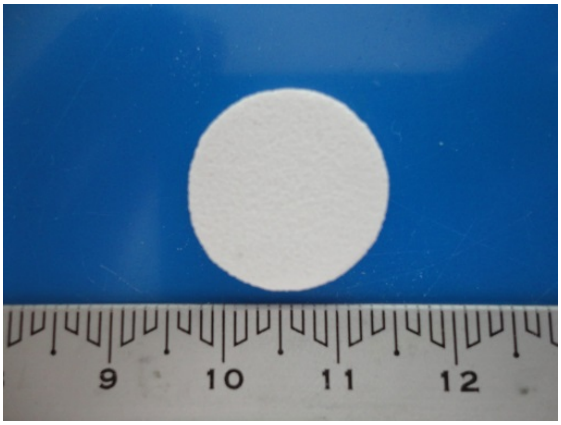

Fig.23b Tablet solution1,preparationA after heat treatment

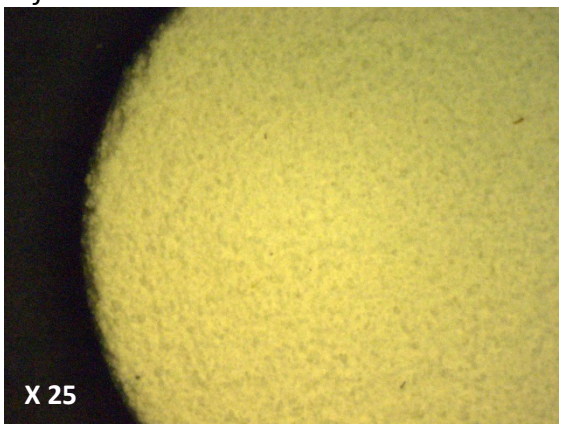

Fig.23c Microscope picture of surface of tablet solution1preparationA

Fig.24a,24b,24c show SEM micrographs of a tablet printed with solution1 (preparation A), after heat treatment.

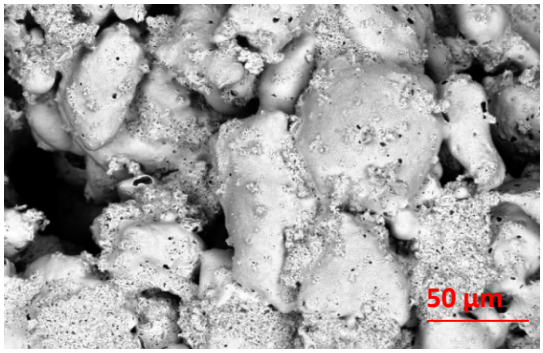

Fig.24a

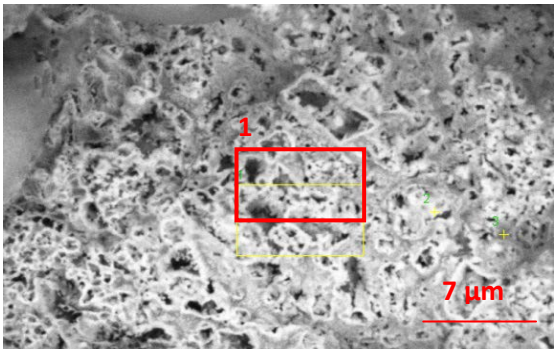

Fig.24b

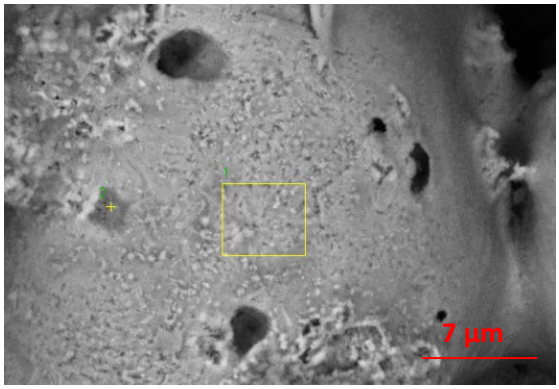

Fig.24a SEM picture of sample solution1, reveal that the particle are sintering. The porosity of the material is evident

Fig.24b SEM picture of sample solution1 in particular reveal that the surface are cristalized showing a porous surface

Fig. 24c SEMpicture of sample solution1 shows on the right size the sintering neck between two AP40 particles.

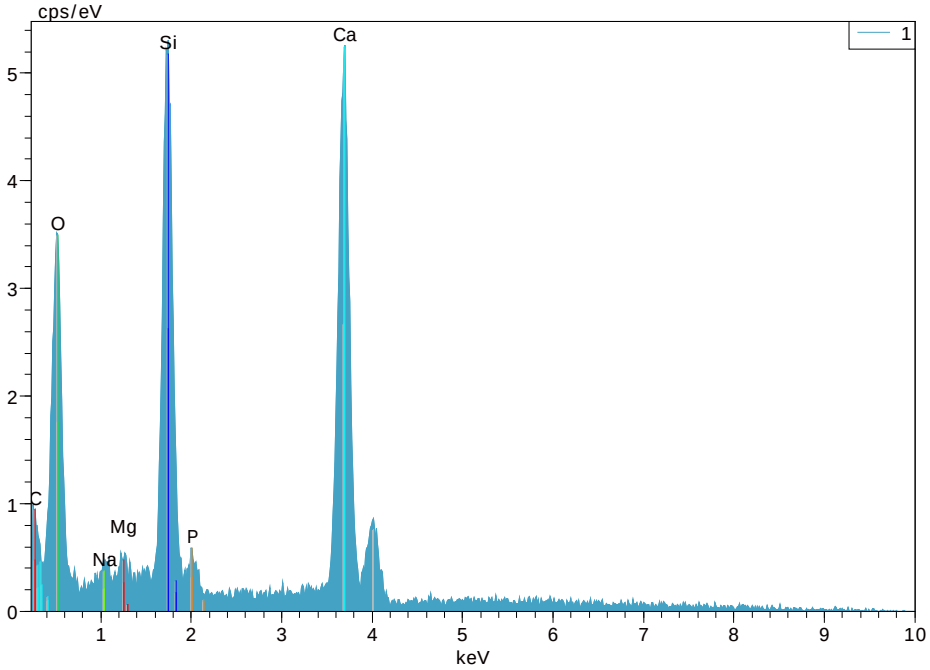

Fig.24d The EDX spectrum of point 1 in fig. 24b revealing the peak of Ca, Si and O

Fig.24a reveals that in the sample after the heat treatment the big particle of AP40 formed sintering necks, though the densification was very limited. Between the AP40 a porous secondary phase is clearly recognizable. The EDX spectrum (point1) relative to this phase, magnified in fig. 24d, shows two peaks of Ca and Si with similar intensities. This phase could be indeed porous wollastonite as expected from the reaction between SiO2 (deriving from the ceramization of MK) and the CaCO3 filler. This observation was also supported by the X-Ray Diffraction analysis(fig.25) of a powdered printed sample.

The extent of densification during sintering of the AP40 particles is probably limited by the coarse dimension of the particles and it might be further hindered by the development of the secondary wollastonite phase observed. It can be noted in fig. 24c that as expected also the surface of the AP40 particles was crystallized.

The X-Ray Diffraction analysis in fig.25 show how the main phases developed after the ceramization process are wollastonite and hydroxylapatite.

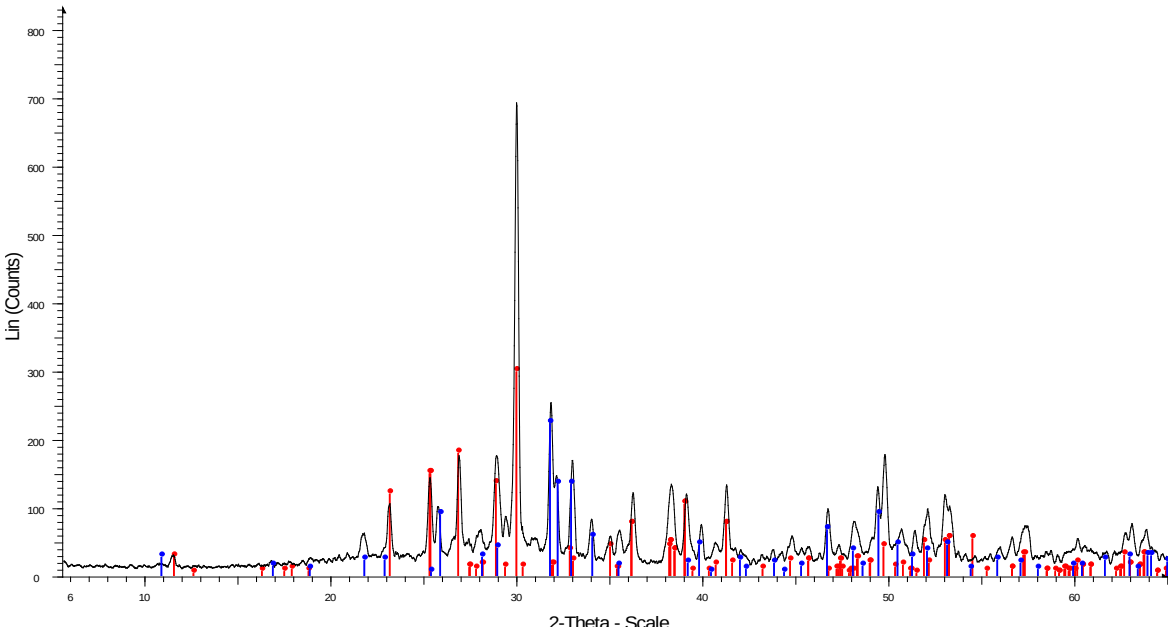

Fig.25 XRD of sample sol1preparationA;the main phases are wollastonite and hydroxylapatite

5.2 Characterization tablets sol2 preparationA

Powder sol.2-preparation A has also been printed with the aim of finding a suitable set of printing parameters, in particular regarding the solvent concentration. It is important to note how it was very difficult to create a layer of powder on the platform due to the poor flowability of this powder; indeed the recoating had to be repeated several times in order to have an entire layer.

Tab.13 shows the dimension of the voxel, the mass of the drop and the mass of the powder in one voxel for five printed samples. From these values, the R value can be calculated using eq. (1).

After several attempts, sample3 could be printed; due to the introduction of more amount of MK powder in this composition, a larger quantity of solvent was used compared to printing of sol1 with the same preparation.

This situation introduced however new complications. The viscosity in sample, just during printing, is lower since there are more MK and more solvent in compared to solution1; in this situation the sample has a higher possibility to deform due to a non-homogeneous solvent distribution and evaporation. This non-homogeneous distribution is facilitated by the non-homogeneous mixing of the raw materials, as depicted in fig.16c. In particular it is expected that the solvent is sucked much easier in

the capillaries formed between the fine $CaCO_3$ particles than in the capillaries between the coarse AP40 particles.
However other tablets like sample3 could be printed for biaxial strength testing and for solution test.
After heat treatment, these samples were heat treated at 900°C / 1h (2°C/min ramp).
The tab.14 shows the average sample dimensions and the shrinkage after ceramization:

	Sample1	Sample2	Sample3	Sample4	Sample5
R	0,062	0,077	0,091	0,111	0,155
Drop mass solvent (ng)	65	65	65	65	65
Powder mass (ng)	1042,6875	834,15	709,0275	583,905	417,075
Delta x (µm)	125	100	85	70	50
Delta y (µm)	83	83	83	83	83
Delta z(µm)	150	150	150	150	150

Table 13 Parameters of printer for tablet solution2

	Average value	Deviation standard
Diam. Green tablet (mm)	15,88	0,23
thickness green tablet (mm)	3,19	0,12
Weight green tablet (g)	0,68	0,04
Diam. ceramized tablet (mm)	14,98	0,15
Thickness ceramized tablet (mm)	3,03	0,13
Weight ceramized tablet (g)	0,53	0,03
Shrinkage diam.	6 %	0,01
Shrinkage thickness	5 %	0,02

Table 14 Average value of tablets printed with solution2 preparationA before and after heat treatment,900°C for 1hour,heating rate 2°C/min, uncontrolled cooling

Porosity and density of the samples were examined like the sample of solution1, in tab.15 are summarized the results of 8 samples. The results are reported in tab 15,all the values are indicated with standard deviation:

Apparent density (g/cm^3)	Geometrical density (g/cm^3)	True density (g/cm^3)	Open porosity	Total porosity
1,19 ± 0,05	0,98 ± 0,04	2,77	0,56 ± 0,02	0,57 ± 0,02

Table 15 Value about density and porosity revealed by Archimedian tecnique

Total porosity is defined by formula (8).
So the samples solution 1&2 (preparation) have similar density and porosity, even though the samples of solution2 type are rather rougher than solution 1 and furthermore the tablet is not printed very precisely.
The fig.26a,26b show the tablet printed with solution 2 preparation A before and after ceramization, the fig.26c show the tablet under microscope.

The photos show the sample of solution2 were more friable, no well-defined and it was impossible to achieve a good accuracy.

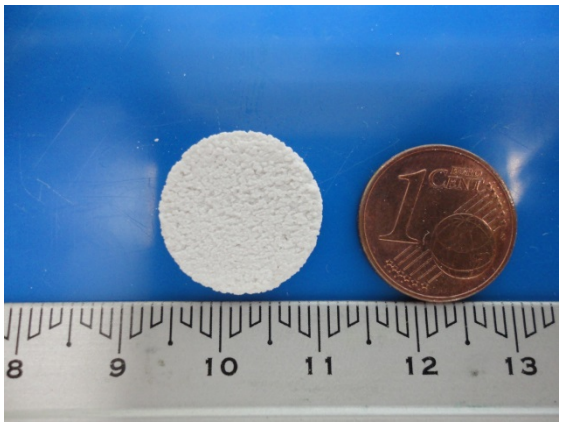

Fig.26a, Tablet solution2 preparationA before heat treatment

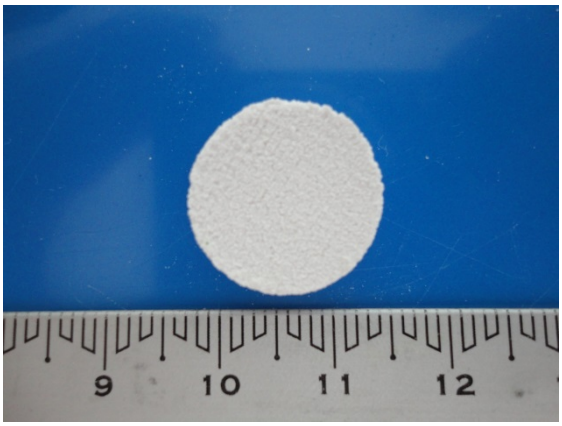

Fig.26b, Tablet solution2 preparationA after heat treatment

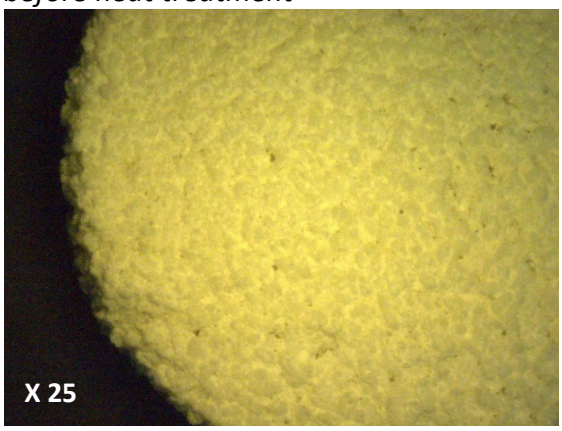

Fig.26c Microscope picture of surface of tablet solution2 preparationA

In fig. 27a,b,c,d the SEM photos of tablet solution2 preparationA

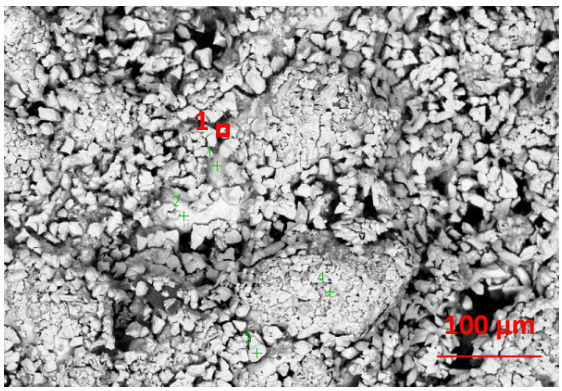

Fig27a SEM pictures of the sample solution2 preparationA after heat treatment reveal big particle that should be from AP40

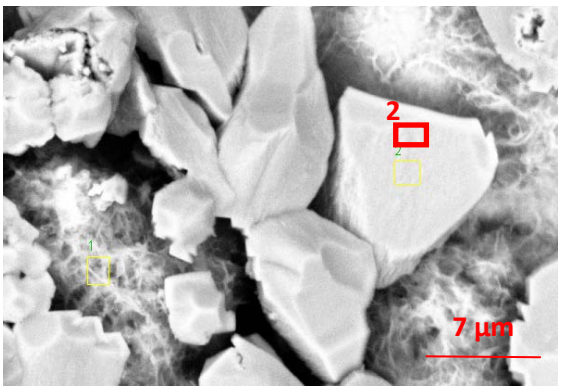

Fig.27b SEM pictures of the sample solution2 preparationA after the heat treatment reveal the small particles from $CaCO_3$

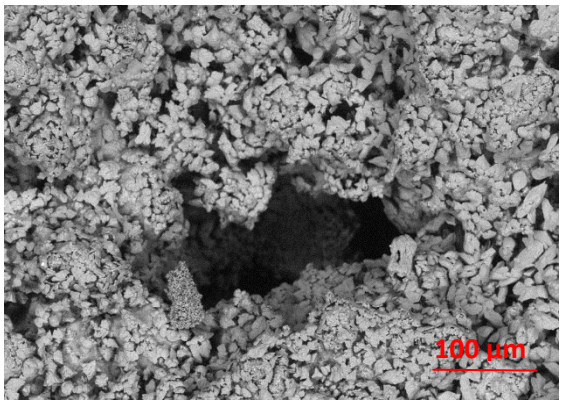

Fig.27c SEM pictures of the sample solution2 preparationA after heat treatment revel a large pore

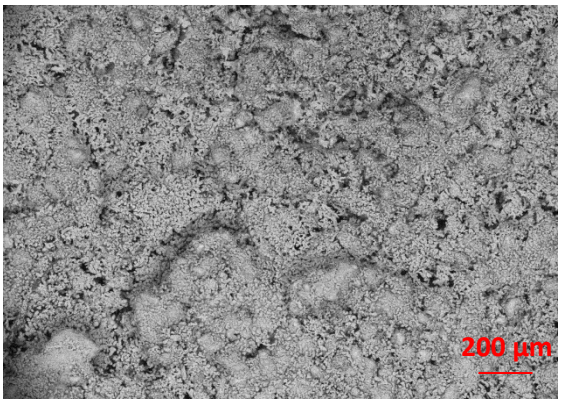

Fig.27d SEM pictures of sample solution2preparationA after heat treatment reveal the presence of aggregate of particles

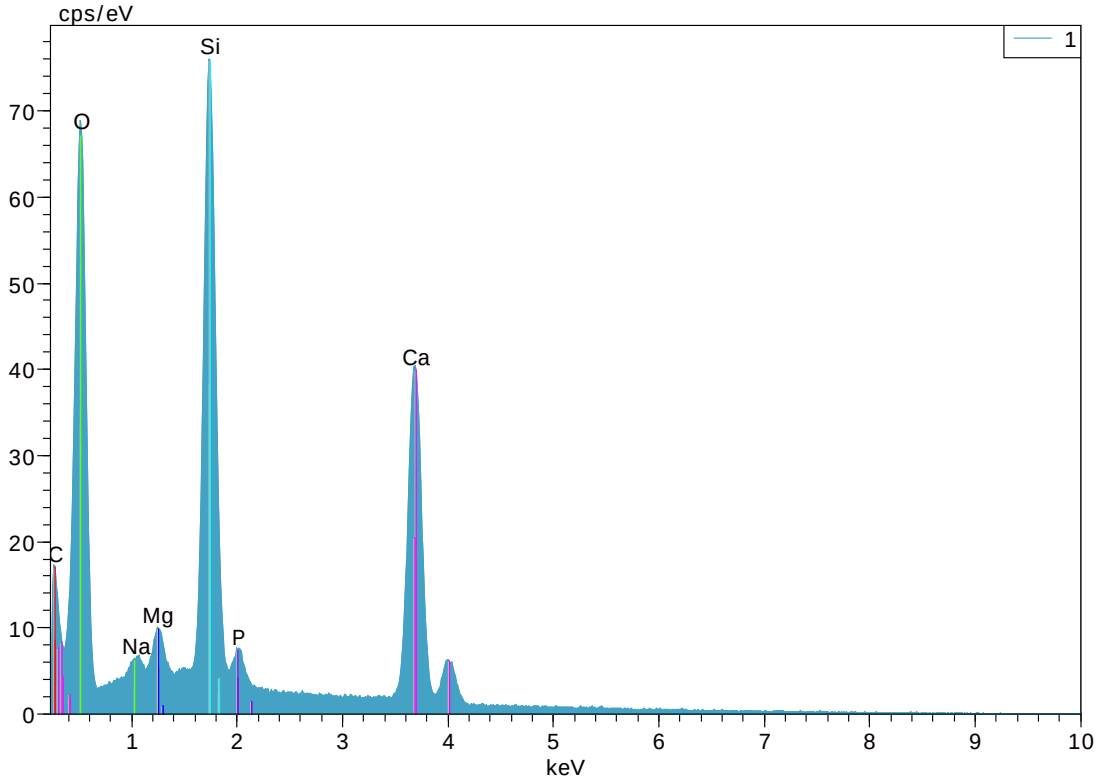

Fig.27e EDX spectrum reveal that the big particles in fig.27a could be from AP40 because there are peaks of Si, O and Ca

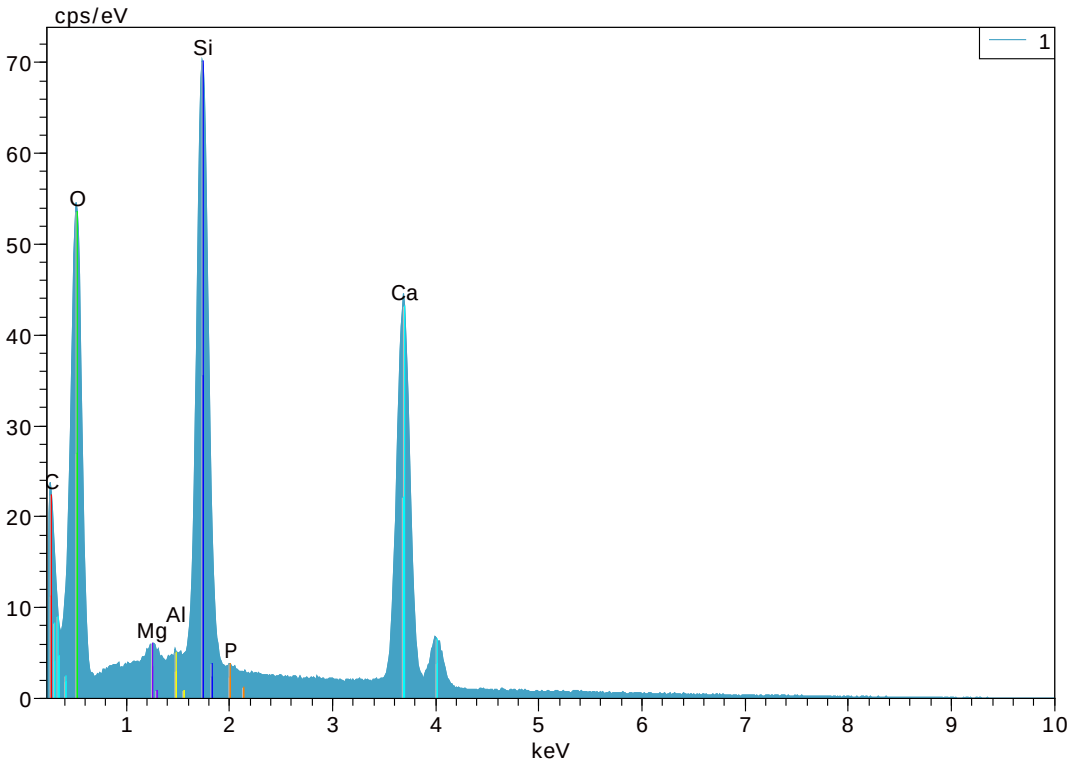

Fig.27f EDX spectrum reveal a peak of Si, O, Ca; in this case maybe there are different phases

In fig.27a the big particles crystallized could be AP40 because in the EDX of point1 in fig.27e there are a peak of Si, O, Ca and a small amount of P and Mg. Fig.27b shows the small particles present is the sample. The EDX spectrum in fig. 27f of point2 reveals main peaks of Si, O, Ca; it seems probable that in this sample other secondary calcium-silicate phases are present, that XRD can reveal. Probably in this sample the phase purity expected could not be obtained during heat treatment, due to a non-homogeneous mixing of the raw materials(fig.27d).

It should be stressed also that some part of the sample's surface shows big pores, such as in fig. 27c, maybe because in these regions there was a high concentration of calcium carbonate and at the same time less particles of AP40.

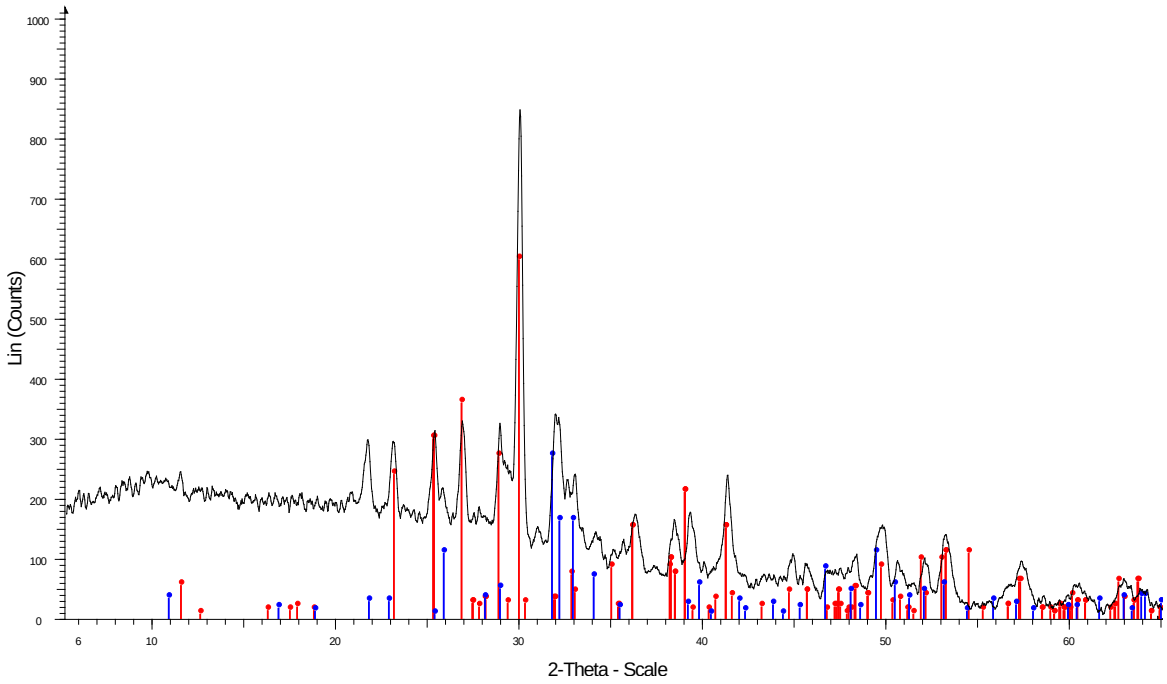

Fig.28 *XRD of sample sol2preparationA;the XRD spectrum reveal the presence of others phases*

5.3 Characterization tablets sol2 preparationB

In order to improve the quality of the samples printed with the solution2, a new preparation method was introduced, named preparation B. As seen previously the flowability of the powder prepared with preparation B was better than preparation A. Following the procedure described in paragraphs 4.1 and 4.2, also with this kind of powder some tablets were printed, first of all looking for the best amount of solvent; was printed with the amount indicated in tab.14 In this case the best tablet was the sample2.

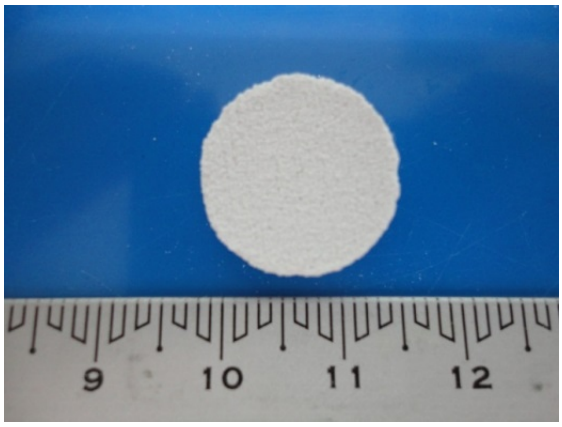

Fig.29a, Tablet solution2,preparationB before heat treatment

Fig.29b, Tablet solution2,preparationB after heat treatment

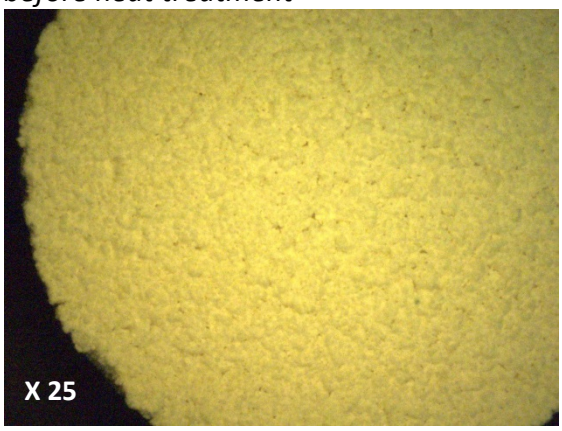

Fig.29c Microscope picture of surface of tablet solution2preparationB

Photo in fig.29a,29b,29c show the samples printed with solution2preparationB;as already anticipated the samples of solution2preparationB reached a good accuracy; the quality and printing precision of these samples are higher than samples of solution2praparationA showed in fig.26a,26b,26c;even thought the tablets of solution1preparationA showed in fig.23a,23b,23c revealed the best quality and accuracy.

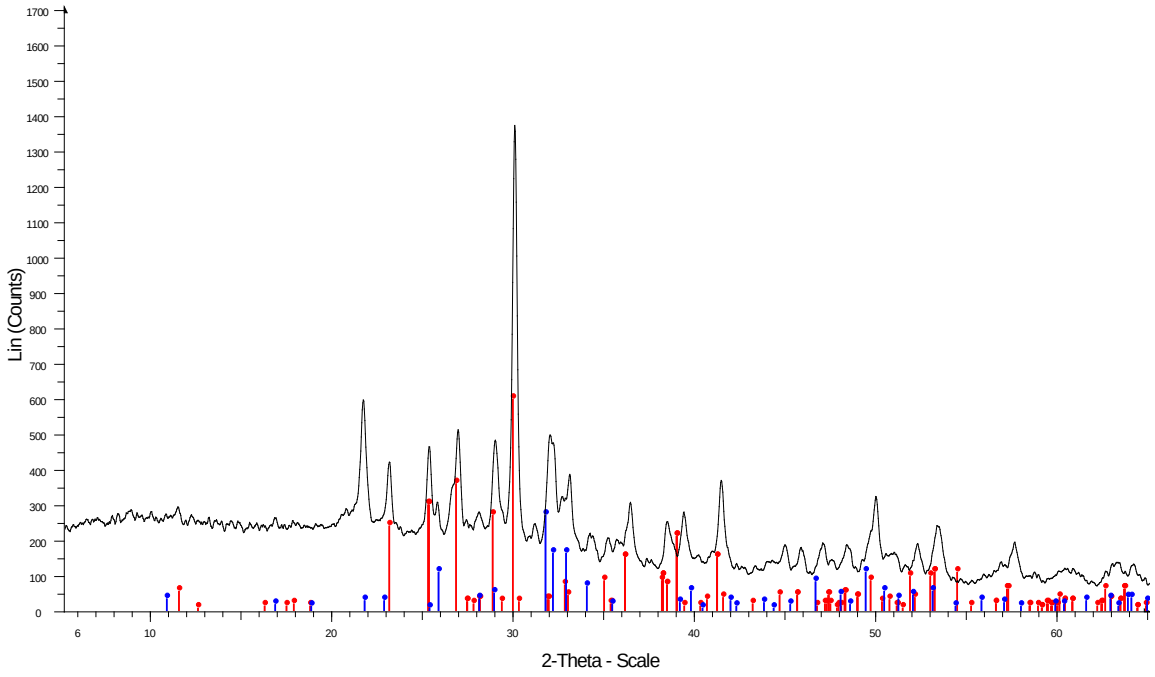

Fig.30 XRD of sample sol2preparationB;the XRD spectrum reveal the presence of others phases

5.4 Solution1 printed and solution1 pressed

It was interesting to analyze the different properties of tablets with different levels of porosity, so printed samples of solution1 and pressed sample of solution1 were prepared and compared..

The samples with low porosity were create using a press, and 16 mm was the diameter of the mould. The samples in this case were pressed in this way:

- once prepared, 0,90 g of powder solution 1 was put into the mould;
- with the machine the powder was pressed until 15 KN;
- this force was maintained for 60 seconds, leaving the time for the particle to glue;
- the sample was extracted from the mold;
- all the sample were enough resistant to be handled;

In the tab.16 the conversion used in order to expess the pressure in MPa:

Force (N)	Sample area (mm^2)	Pressure (N/mm^2=MPa)
15000	201,0	74,7

Table 16 Value of force and pressure used for pressing the samples.

The characteristics of the printed samples has already been reported in tab.11, in tab.17 were written the data about the pressed sample:

	Average value	Deviation standard
Diam. Green tablet (mm)	16,09	0,03
thickness green tablet (mm)	2,69	0,08
Weight green tablet (g)	90,0	0,00
Diam. ceramized tablet (mm)	15,56	0,03
Thickness ceramized tablet (mm)	2,78	0,06
Shrinkage diam.	3 %	0,00

Table 17 Average value of tablets pressed with solution1 before and after heat treatment,900°C for 1hour,heating rate 2°C/min, uncontrolled cooling.

In this case there is a slight shrinkage of the tablets after ceramization process and the porosity is quite big, around 40 % although does not reach the same value of printed samples. The shrinkage is not high like printed samples probably because the release of gas creates additional porosity.
Porosity and density of the pressed samples were examined like the printed samples of solution1 and solution2, in tab.18 are summarized the results of 8 samples. The results are reported in tab 12,all the values are indicated with standard deviation:

Apparent density (g/cm^3)	Geometrical density (g/cm^3)	True density (g/cm^3)	Open porosity	Total porosity
1,63 ± 0,01	1,52 ± 0,03	2,77	0,39 ± 0,01	0,41 ± 0,01

Table 18 Value about density and porosity revealed by Archimedian tecnique

The lower apparent porosity suggests a higher value of biaxial flexure strength compared to printed sample with a higher porosity, anyway the result about mechanical test will be explain in the paragraph “Biaxial flexural test”.

5.5 Solution1 Preparation B

This paragraph is entirely dedicated to tablet and others samples printed with solution1 preparationB. As already stated, the first powder preparation method was not completely acceptable; consequently, new powder of sol1 with preparation B was created. This powder was more flowable and the layers in the 3D-printing machine could be recoated easier.
A good flowability for a powder is an important result but it is not the only requirement. Indeed it is important to the quality of the sample printed, his resolution and good accuracy of the sample. It was seen that the overall quality of the samples printed with solution1 was higher than solution2 and furthermore also preparation B

gave better results than preparation A. Based on these results, tablets were printed with a powder solution1 prepared with method B.
The first step was to find out the correct amount of solvent. In tab.19 are summarized the different attempts:

	Sample1	Sample2	Sample3	Sample4
R	0,053	0,066	0,094	0,132
Drop mass solvent (ng)	59,9	59,9	59,9	59,9
Powder mass (ng)	1137,6	910,1	637,1	455,0
Delta x (µm)	125	100	70	50
Delta y (µm)	83	83	83	83
Delta z (µm)	150	150	150	150
	Sample5	**Sample6**	**Sample7**	**Sample8**
R	0,165	0,219	0,263	0,411
Drop mass solvent (ng)	59,9	59,9	59,9	59,9
Powder mass (ng)	364,0	318,5	273,0	227,5
Delta x (µm)	40	30	25	20
Delta y (µm)	83	83	83	83
Delta z (µm)	150	150	150	150

Table 19 Parameters of printer for tablet solution1 preparationA;

The tab.20 show the different tablets printed:

Sample1 Sample2 Sample3 Sample4 Sample5 Sample6 Sample7 Sample8

Table 20 Eight samples printed in order to discovered the right amount of solvent

In tab.20 the different samples are show; obviously samples 1,2,3 were printed with not enough solvent, and so the tablets were damaged because the solvent was insufficient to dissolve all the MK and bind the particles; consequently some powder was not attached and the tablets were imperfect.
Samples 6,7,8 were the best, even if for these samples it was more difficult to remove the surrounding unbound powder. Indeed when a large amount of solvent was employed, a small part of it can flow out from the shape of the sample, attaching weakly the neighboring particles. At the end the best sample was the last one with the greatest amount of solvent (sample 8).
Once found the right parameters to print non-macro porous samples, it was interesting to analyze how to print samples containing an ordered porosity with powder solution1,

preparationA. The next step of the research was to print a grid with different dimensions of macro pores and struts.

Fig.31a,31b, show the different grills printed, and tab. 21 shows the different R ratio employed.

	Grid1	Grid2	Grid3	Grid4
R	0,172	0,196	0,229	0,229
Drop mass solvent (ng)	62,5	62,5	62,5	62,5
Powder mass (ng)	364,0	318,5	273,0	273,0
Delta x (µm)	40	35	30	60&60=30
Delta y (µm)	83	83	83	83
Delta z (µm)	150	150	150	150

Table 21 Parameters of grid for tablet solution1 preparationA;

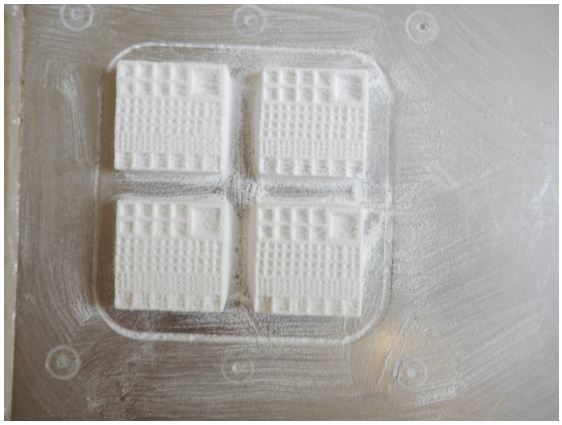

Fig.31a The four grids on the platform

Fig.31b The four grids on the platform

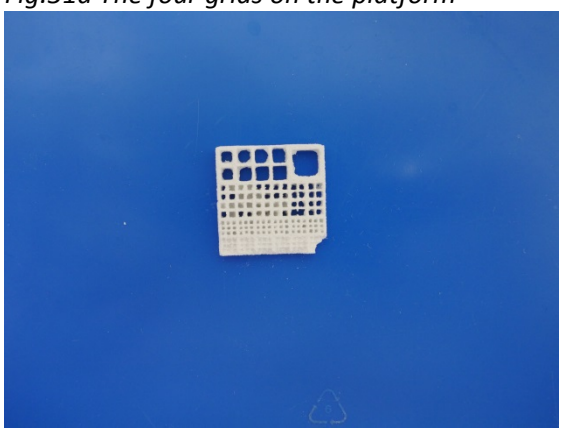

Fig.31c Picture of grid 1

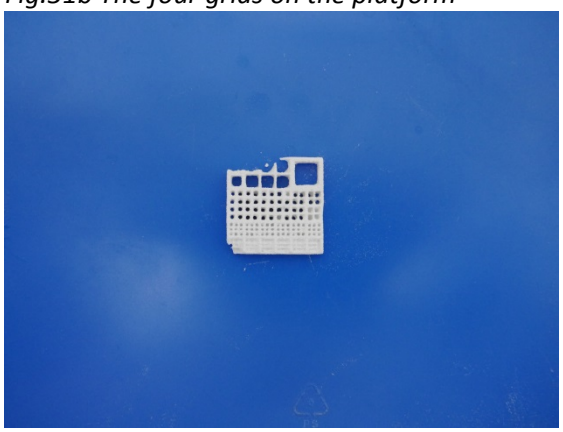

Fig.31d Picture of grid 2

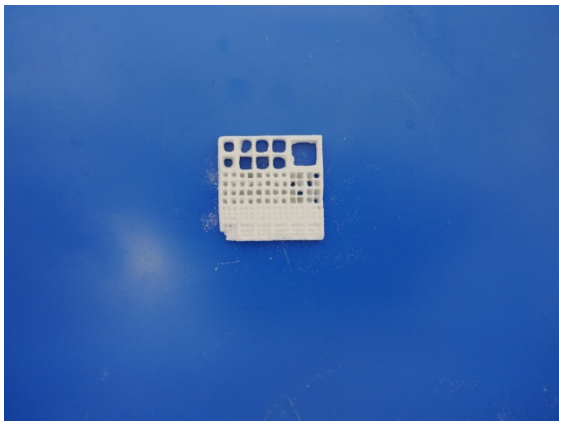

Fig.31e Picture of grid 3

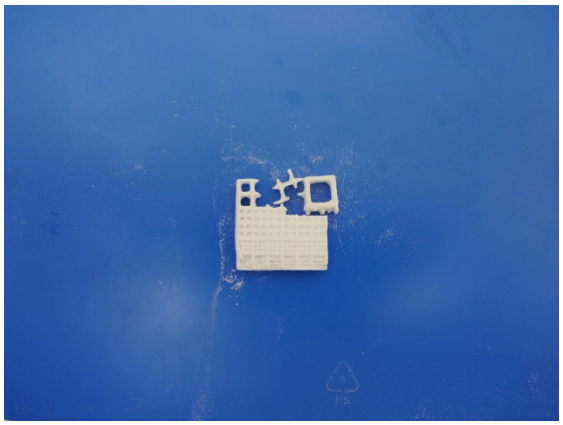

Fig.31f Picture of grid 4

Fig.31a,31b show how the samples seem similar. Anyway while removing the powder the grids broke a certain point because the struts were too weak (fig.31c,31d,31e,31f).
It is important to emphasize that grid4, it was printed in a different way; indeed a $\Delta x = 60$ µm was used, but in this case the printing was repeated twice for each layer. The amount of solvent introduced was equivalent to a $\Delta x = 30$ µm, but with the difference that the solvent has a little time to partially evaporate between the two repetitions.
The final step of the research was the printing of some scaffolds; these scaffolds were printed based on the images shown in fig.8b,8c. They are macro-porous cubes with these dimensions: 10mmx10mmx10mm. Fig.34 shows the printed scaffolds; the first attempt was to print 16 scaffolds, all in the same platform; this means that the scaffold were very close each other. These scaffolds were printed with the parameters shown in tab.22

	scaffolds
R	0,219
Drop mass solvent (ng)	59,9
Powder mass (ng)	273,5
Delta x (µm)	30
Delta y (µm)	83
Delta z (µm)	150

Table 22 Parameters of printer for the grid sample with soluiton1 preparationB

So the amount of solvent was very similar to grid 3; the scaffolds are shown in fig.34

Fig.32 Scaffolds printed on the platform

As fig.32 shows the powder close to the scaffold was also partially connected, and so it was a little more difficult to remove it. Indeed main problem was to remove the unbound powder. Part of the scaffolds was damaged during cleaning, but some of them could be successfully produced as in fig.33a,33b.

Fig.33a Scaffold printed with soutionl1preparationA

Fig.33b Scaffold printed with solution1 preparationA

CHAP.6 CHARACTERIZATION OF SAMPLES

6.1 Biaxial flexural strength

The ball on three balls test for strength testing was used to check the mechanical behavior of the tablets (50)(51).
This test is claimed to have some benefits compared to uniaxial testing, for example: the much simpler specimen preparation, the avoiding of tensile loaded edges, the similarity of stress state to those from typical loading and surely, the biaxial stress state are more revealing of defects than uniaxial stress states. In this test the tablet is supported by three balls and then axially loaded from the opposite side via a fourth ball.
Especially, small deviations from the requested geometry usually are tolerable, but threefold bending symmetry makes extremely difficult an exact analytical assessment of the stress state in the loaded disc.
The loading velocity used was: 0,01 mm/sec. The maximum stress in the sample was calculated from the maximum force applied based on the equation that can be found in this article (52). The formula considers the diameter and the thickness of the samples and the Poisson's ratio of the material.
It should be stressed that the Poisson's ratio is influenced by the porosity of the material; in particular the Poisson's ratio value of isotopic porous materials with spherical pores is obtained from this formula: (53).

$$v_P = \frac{0{,}5-\left(1-P^{\frac{2}{3}}\right)^{1{,}21}}{4\left[(1-s)\frac{(3-5P)(1-P)}{2\,(3-5P)(1-2v_0)+3P\,(1+v_0)}\right]+s\,\frac{s(1-P)}{3(1-v_0)}} \quad (9)$$

With:

$$s = \frac{1}{1+e^{-100(P-0{,}4)}} \quad (10)$$

v_P is Poisson's ratio of porous material, P is the porosity of the material, v_0 is the Poisson's ratio of the dense material, v_0=0,27,indicated in the article(54),where the Poisson's ratio of Apatite/Wollastonite material is v_0=0,27.
For solution1,preparationA the porosity of the material is: 0,61
For solution2,preparationA the porosity of the material is: 0,56
So using the formula(9),v_P for solution1 is 0,40 and for solution2 is 0,31.
For ceramic materials the most important drawback is their brittleness. For this reason it is difficult to predict the ultimate strength of the materials because this value may be

vary from specimen to specimen, even under identical testing conditions. This is related to the distribution of flaws in body or in the surface of the material, since the failure processes start from the flaws.
The Weibull distribution is the model most frequently used to describe the ultimate strength of ceramic material, therefore this model has been used in this research, using the formula:

$$lnln\frac{1}{S} = mln\frac{\sigma}{\sigma_0} = mln\sigma - mln\sigma_0 \quad (11)$$

The Weibull modulus m, is a shape parameter for the Weibull distribution model which maps the probability of failure of the sample at varying stressing.
In this case has been considered Sj, probability of survival, and was used in this formula:

$$S_j = 1 - \frac{j-0,3}{N+0,4} \quad (12)$$

j is j-esimo sample and N is the number of all samples; so it is possible to draw a graph, plotting in the x-axis $ln\sigma$ and in y axis $lnln1/S_j$. Tab.23 shows the value for every sample.

σ (MPa)	Sj	Ln(σ)	Ln(ln(S_j))
3,440	0,917	0,850	-2,44172
3,140	0,798	0,971	-1,48667
2,340	0,679	1,078	-0,94735
2,640	0,560	1,078	-0,54357
5,640	0,440	1,144	-0,19857
3,140	0,321	1,144	0,126615
2,940	0,202	1,235	0,468505
2,940	0,083	1,730	0,910235

Table 23 Parameters obtained from biaxial flexural strength for sol1 printed, used to derive the Weibull modulo, the data are plotted in the graph represented in fig.33

From the graph it is possible to obtain the Weibull modulus from the slope of the interpolating line and (55)σ_0 from the formula:

$$S = \exp\left[-\left(\frac{\sigma}{\sigma_0}\right)^m\right] \quad (13)$$

S=1/e=0,37.
Fig.34 shows the Weibull graph for sample solution1, preparation.
One of the points (in red), which was out of regression trendline, has been excluded; the equation in the right part of the graph was calculated without the value of this sample.
From the slope of the interpolating line, a Weibull modulus, m =7,78 and σ_0=3,20 MPa from formula (13) could be calculated.

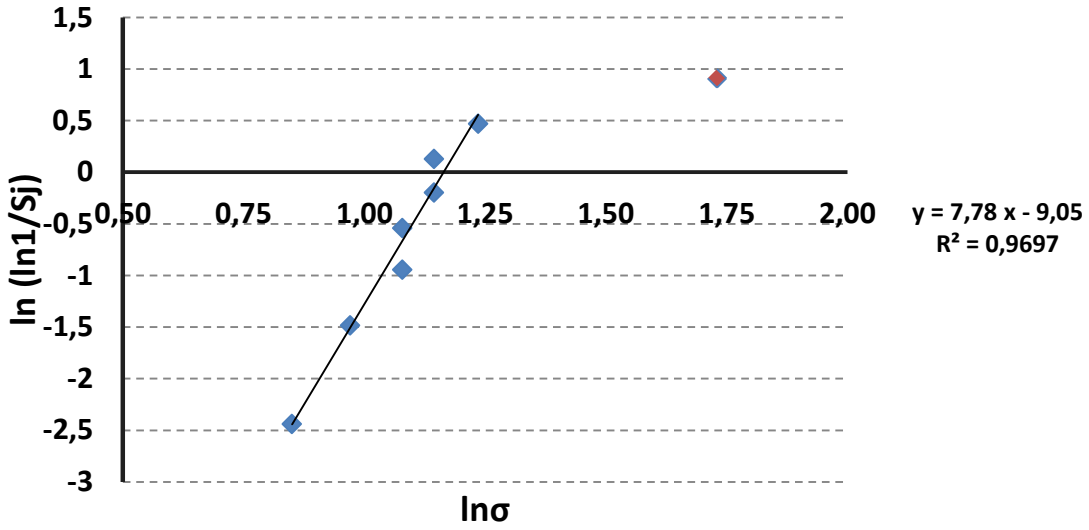

Fig.34Weibull plot,ln(ln1/Sj) vs lnσ of printed samples solution1preparationA. The graph reveal the Weibull modulo m= 7,78,and σ_0=3,20MPa. The samples follow the same trend except one sample

Also for the sample solution2 was calculated the same values. The tab.24 revealed the values :

σ (MPa)	Sj	Ln(σ)	Ln(ln(S_j))
2,1	0,92	0,74	-2,44
2,44	0,80	0,89	-1,49
3,14	0,68	1,14	-0,95
3,34	0,56	1,21	-0,54
4,18	0,44	1,43	-0,20
4,24	0,32	1,44	0,13
4,58	0,20	1,52	0,47
4,84	0,08	1,58	0,91

Table 24 Parameters obtained from biaxial flexural strength for sol2 printed, used to derive the Weibull modulo, the data are plotted in the graph represented in fig.34

The fig.35 shows the Weibull distribution for sample2,preparationA.

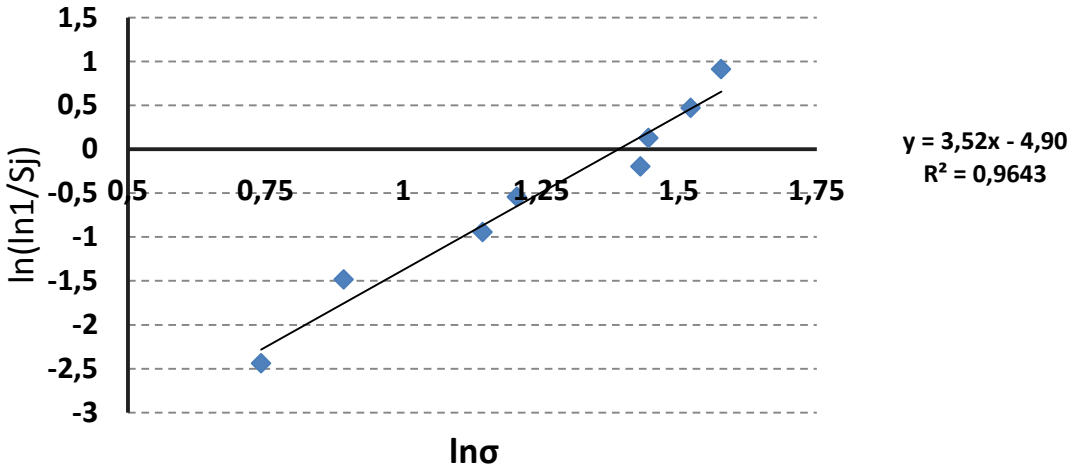

Fig.35Weibull plot,ln(ln1/Sj) vs lnσ of printed samples solution2preparationA. The graph reveal the Weibull modulo m= 3,52 and σ_0=4,02MPa. The samples follow the same trend

In this graph the value of Weibull modulus is different, is value 3,52 and σ_0=4,02 MPa, it is interesting to compare this value with the Weibull modulus of sample solution1. Indeed in this last case the modulus is smaller than for sample solution1, and so the measurements show a larger variation from sample to sample. It may be concluded that in this case the defects in the material, such as the porosity resulting from the manufacturing process, is distributed less uniformly throughout the material.

As previously anticipated it is interesting to compare the printed porous samples of solution1 with pressed sample produced with solution1. The tab.25 reveal the value for the sample of solution1 preparation A

σ (MPa)	Sj	Ln(σ)	Ln(ln(S_j))
4,54	0,96	1,51	-3,13
22,48	0,90	3,11	-2,21
22,78	0,84	3,13	-1,72
23,52	0,77	3,16	-1,36
23,62	0,71	3,16	-1,09
23,78	0,65	3,17	-0,85
23,92	0,59	3,17	-0,64
24,72	0,53	3,21	-0,46
24,72	0,47	3,21	-0,28
25,76	0,41	3,25	-0,11
25,92	0,35	3,26	0,06
25,95	0,29	3,26	0,22
26,12	0,23	3,26	0,40
26,62	0,16	3,28	0,59
27,56	0,10	3,32	0,82
32,44	0,04	3,48	1,15

Table 25 Parameters obtained from biaxial flexural strength for sol1 pressed, used to derive the Weibull modulo, the data are plotted in the graph represented in fig.35

Tab.25 shows the elaboration of the Weibull statistic for pressed samples of solution1 preparation A.Fig.36 shows the Weibull distribution for pressed sample solution1 preparationA.

.

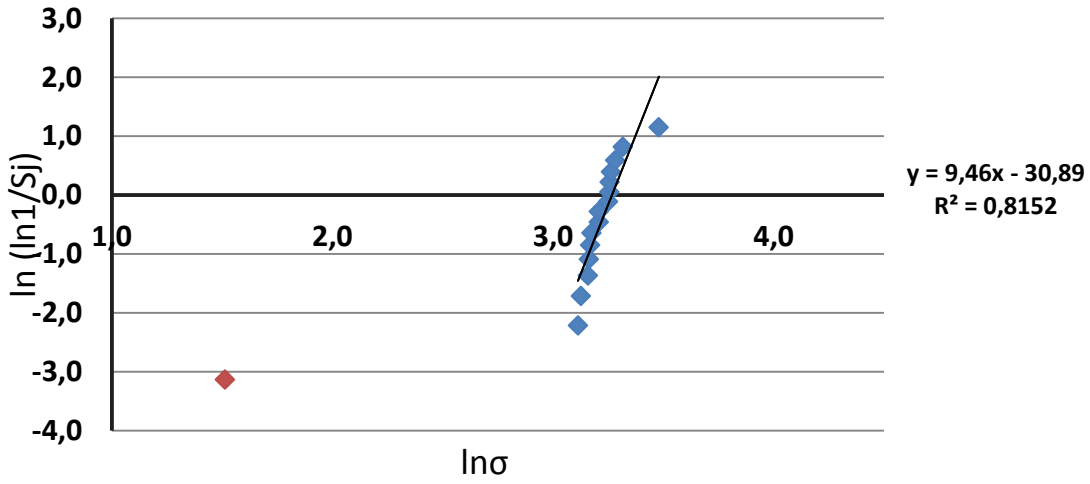

Fig. 36 Weibull plot,ln(ln1/Sj) vs lnσ of pressed samples solution1preparationA .The graph reveal the Weibull modulo m= 9,46 and σ_0=26,20 MPa . The samples follow the same trend except one sample

In this case m=9,46 and σ_0=26,20MPa. One of the points (in red), which was out of regression trendline, has been excluded.
The main difference between printed and pressed samples is the σ_0 value that is higher for the pressed sample (σ_0 =26,18) compared to printed sample(σ_0 =4,02); that is quite obvious, indeed the porosity is 39 % compare to 61 % of printed sample; an increased porosity generally influences negatively the mechanical properties of the material.

6.2 Solubility test

A solubility test was performed on selected samples, printed and pressed.
Tab.26 shows the average weight and the composition of the prepared samples:

Number	Average Weight (g)	solution	note
4	0,846	Sol1	Printed
4	0,763	Sol2	Printed
3	0,863	AP40 (45-90 µm)	Pressed
3	0,197	Woll (0-45 µm)	Pressed
3	0,783	Sol1	Pressed
3	0,686	Sol2	Pressed
3	0,850	AP40 (45-90 µm)	Printed
3	0,565	Woll	Printed

Table 26 Tablets made for solubility test

The solubilities were determined according to DIN EN ISO 10993-14.

At least 3 samples Tris -HCl buffer solution (pH (37°C) = 7.4) for each material were weighed (tablets) and with the appropriate amount (20ml for 1g , 10ml for 0,5g) was added in treatment vessels . The treatment vessels then were stored for 120 h at 37 ° C with circular movements in the incubator. Afterwards , the solutions were decanted and centrifuged (3500rpm for 2min) and 50 or 25ml transferred .

Then, the treatment vessel (containing sample) was washed 2x 0.1 M TRIS - HCl buffer and centrifuged again with 2.5 ml and added to the solution in the volumetric flask . The flasks were then filled with e-pure H2O. To prepare the test solutions 5ml 10ml aliquots were used. The solubilities of the elements were determined by ICP -OES Optima 3,000. After 120 hours test , the solutions were taken weekly for 10 weeks in the same manner and measured. The samples were mixed with fresh TRIS -HCl buffer solution in an appropriate amount and stored in the incubator for the next week .

The dissolution behavior of the different samples presented in tab.26 was evaluated. Ca and Si released from the different samples during the ten weeks are shown in fig. 37 and fig. 38. In fig. 39 are analyzed the release of this ions: Ca, K, Mg, Na, PO_4, Si, Zn.

From the fig.37 it can be seen the release of Ca has the highest value in the samples containing only Wollastonite; furthermore sol2, which has theoretically a higher amount of wollastonite than sol1 (60wt% and 20wt% respectively), has a higher release of Ca than sol1.

Furthermore, generally the solubility is higher for printed samples than for pressed samples, as expected because of the higher porosity in the printed samples.

The release of Si in fig.38 is more similar for the different types of samples, and follows a linear trend.

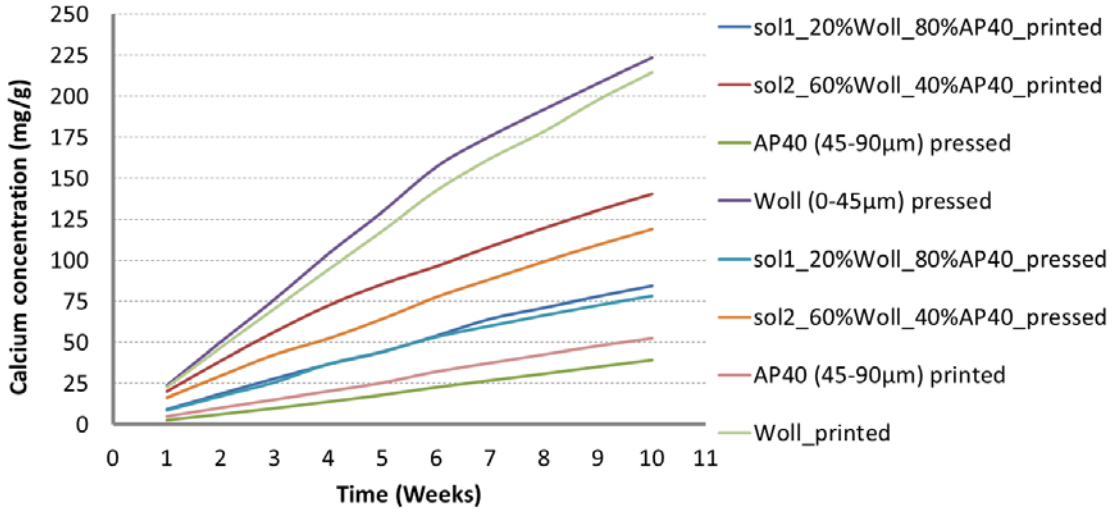

Fig.37 Calcium concentration release from the different tablet during tris-HCl test during the ten weeks

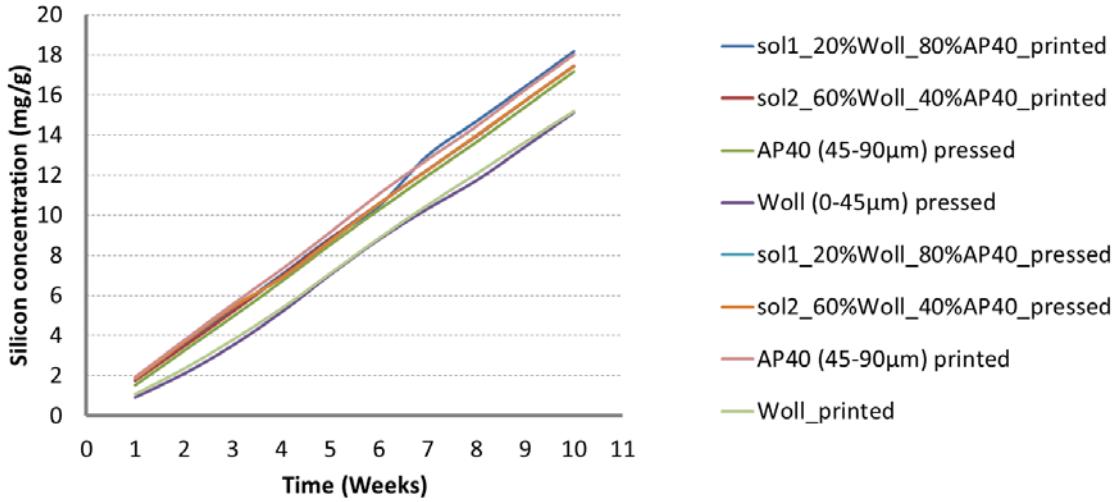

Fig.38 Silicon concentration release from the different tablet during tris-HCl test during the ten weeks

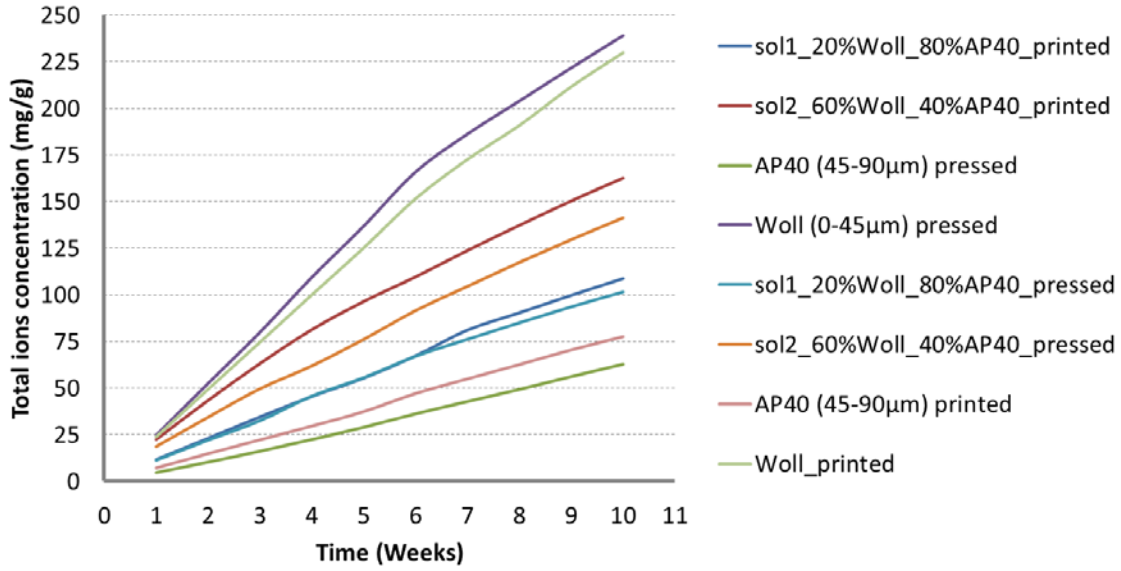

Fig.39 Total ion concentration release from the different tablet during tris-HCl test during the ten weeks

In the fig.39 the release of all ions considered follow the trend of Ca, indeed there is more release for samples made with wollastonite; for example also in this case the samples made with solution2 release more ions than solution1, surely linked at the amount of wollastonite.

6.3 Biological in-vitro evaluation

Samples of sol1 preparationA and sol2 preparationB were printed for biological in-vitro tests. The average diameter of the samples was 10,42 mm for sol1 and 10,12 mm for sol2, and the thickness 2,50 mm for sol1 and 2,48 mm for sol2 after ceramization.
The samples before the test were sterilized at 300 °C for 3 hours; after they were placed in usual cell culture medium for 24 hours.
Then medium was removed and a specific amount of cell was seeded on the top of the samples, i.e. 50000 cells per sample. Cells were allowed to attach for 2 hours and then were filled with medium again.
The assays performed were the Alamar Bleu® (viability), CellTox Green (toxicity) and Caspase 3/7 (apoptosis) assays. Samples were observed by scanning electron microscopy (SEM) for morphology.
Samples were evaluated at 3,7 and 14 days.
After 14 days of incubation in medium the material sol1 did not presented important changes in morphology (Fig.40*a,40*b).
Sol2 presented two different morphological aspects after the incubation period: one more similar to sol1, showing a morphology with more rounded particles; the other

aspect is a more discontinuous structure, due to the presence of acicular structure. These crystals got thicker with the immersion time in medium (Fig.40*c,40*d).

(* in collaboration with Marco A.Lopez,Faculty of Dentistry,Philipps Universitat)

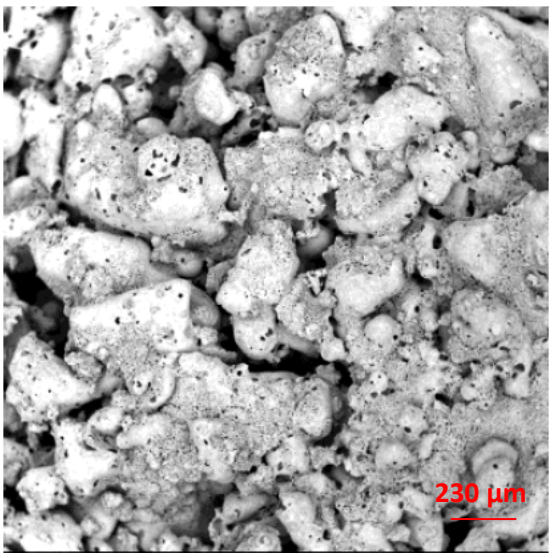

Fig.40 a SEM picture show the morphology of sample solution1 before incubation in medium.

Fig.40 b SEM pictures show the morphology of sample solution1 after 14 days of incubation in medium; the morphology is similar

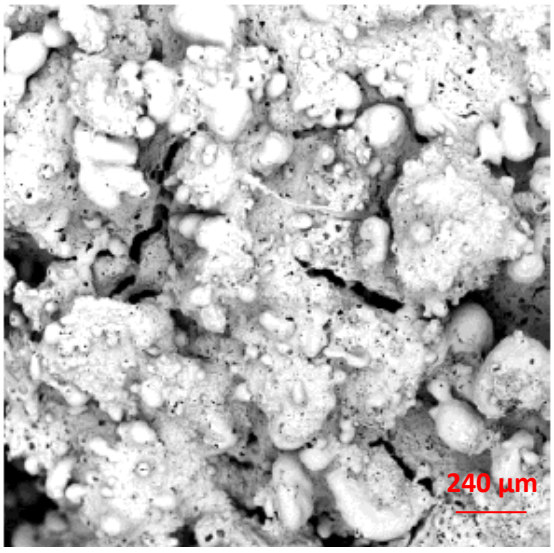

Fig.40 c SEM picture show the morphology of sample solution2

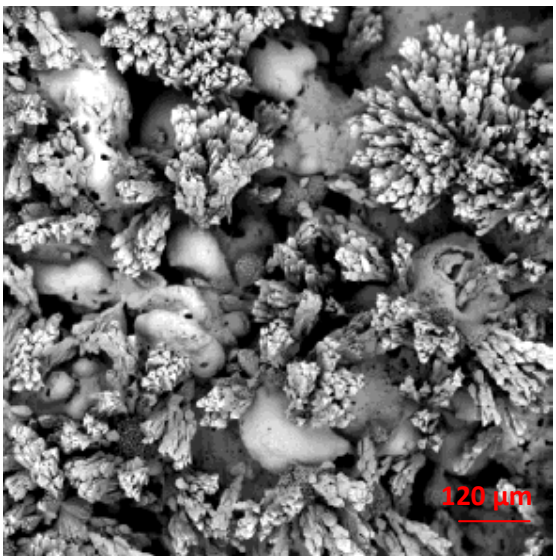

Fig.40 d SEM picture show the acicular crystals morphology of sample solution2 after 14 days of incubation in medium.

Fig. 41*a,41*b show the growth of the cells after 14 days. In both materials at the initial time points some cells were observed, this increased after 7 days and by the latest time point a full cells coverage has been observed.

Fig.41a SEM pictures of surface of sample solution1 after 14 days show the growth of cells

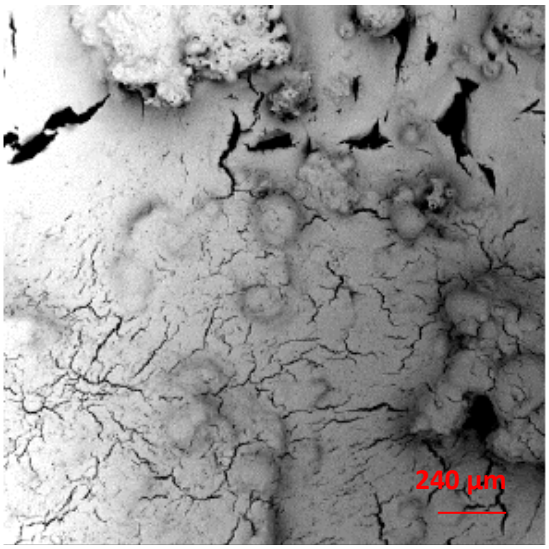

Fig.41b SEM pictures of surface of sample solution2 after 14 days show the growth of cells

(* in collaboration with Marco A.Lopez,Faculty of Dentistry,Philipps Universitat)

From this results it could be said that the material presented different overall morphologies related to their compositions, anyway on both materials the cell growth well. The materials were no toxic to them and the apoptotic signaling is highly probably related to the cell behavior.

CHAP.7 CONCLUSIONS

Two different solutions have been investigated for the powder-based three dimensional printing process. Both solutions are composed of a preceramic polymer filled with two different fillers: a bio glass-ceramic (AP40), and calcium carbonate.
AP40 was inserted as “passive filler” because it does not react with the preceramic, while $CaCO_3$ as “active filler”, because the CaO deriving from the decomposition of CaCO3 reacts chemically react with SiO_2 deriving from the preceramic polymer, to form wollastonite. The solutions have two compositions with a different amount of AP40:

- Solution 1: 20 % Wollastonite (MK + $CaCO_3$) , and 80 % Glass (AP40)
- Solution 2: 60 % Wollastonite (MK + $CaCO_3$), and 40 % Glass (AP40)

Once noticed that the first technique (preparationA) to prepare the solutions was inadequate, especially for the second solutions, a new strategy (granulation of the raw materials, preparationB) was introduced conducting to good results, particularly for solution 1.
Furthermore with solution2 it was impossible to achieve good printing results, probably due to a large amount of fine $CaCO_3$ particles.
However the tablets printed with solution1 and solution2 had similar porosity after heat treatment, respectively 61% and 56%.
The Biaxial flexural strength test showed two different Weibull moduli for the two solutions: indeed for solution1 is m=7,78 and for solution2 is m=3,52 highlighting how in the tablets of solution2 the porosity and defect are not distributed uniformly throughout the material. Moreover, the mechanical strength of pressed samples was higher compared to porous printed materials.
The Tris -HCl buffer solution test showed that the samples with large amount of wollastonite release a large amount of Ca and Si. Biological in-vitro tests for solution1 and solution2 showed that the printed materials were not toxic and that the cells could grow well after 14 days.
In addition to this the printability of solution2 has been checked trying to print this solution, once without $CaCO_3$ and the other without AP40. In first case the sample show a good quality, demonstrating a good accuracy of the samples; without AP40 on the other hand the samples show the same problem presented for solution2,probably due of calcium carbonate.

Bibliography

(1) L. L. Hench, I. Thompson ,"Twenty-first century challenges for biomaterials",2010, J.R. Soc.Interface.

(2) M. Pettinicchio, R. Sammons ,S. Caputi, A. Piattelli,T. Traini,"Bone regeneration in sinus augmentation procedures with calcium sulphate. Microstructure and microanalytical inestigation",2012.

(3) L.L. Hench,J.Wilson "Surface active biomaterials",1984.

(4) Ian Gibson, David W.Rosen, Brent Stucker "Additive Manufacturing Technologies: Rapid Prototyping to Direct Digital Manufacturing"

(5) J.-P. Kruth, M.C.Leu, T.Nakagawa "Progress in additive manufacturing and rapid prototyping"

(6) Griffith, M.L. & Halloran, J.W. (1996) " Freeform fabrication of ceramics via sterolithography " ,J. Am. Ceram. Soc.,79, 2601-2608.

(7) X. Zhang, X.N Jiang, C. Sun, "Micro-stereolithography of polymeric and ceramic microstructures", 1999.

(8) Charlers W. Hull (1986)"Apparatus for production of three-dimensional objects by stereolithography"

(9) Iwan Zein, Dietmar W. Hutmacher, Kim Cheng Tan, Swee Hin Teoh, "Fused deposition modeling of novel scaffold architecture for tissue engineering applications",2001.

(10) Samar Jyoti Kalita, Susmita Bose, Howard L. Hosick, Amit Bandyopadhyay "Development of controlled porosity polymer-ceramic composite scaffolds via fused deposition modeling"

(11) Paul Calvert "inkjet printing for materials and device",2001.

(12) Veronica Sanchez-Romaguera, Marie-Beatrice Madec, Stephen G. Yeates "Inkjet printing of 3D metal-insulator-metal crossovers"

(13) A. Butscher, M.Bohner ,S. Hofmann, L.Gauckler, R. Muller "Structural and material approaches to bone tissue engineering in powder-based three-dimensional printing"

(14) Mukesh Agarwala, David Bourell, Joseph Beaman, Harris Marcus, Joel Barlow "Direct selective laser sintering of metals"

(15) J.P. Kruth, X.Wang, T. Laoui, L. Froyen "Lasers and materials in selective laser sintering"

(16) D. Klosterman,R.Chartoff,G. Graves, N. Osborne, B.Priore,"Interfacial characteristics of composites fabricated by laminated object manufacturing", 1998,Pages.1165-1174

(17) Chyntia M. Gomes,Antonio P.N. Oliveira, Dachamir Hotza, Nahum Travitzky, Peter Greil, "LZSA glass-ceramic laminates: Fabrication and mechanical properties"

(18) Gomes, C.M., Travitzky, N., Greil, P., Oliveira, A.P.N., Hotza, D., Laminated Object Manufacturing (LOM) of glass ceramic substrates for LTCC applications, in Innovative developments in design and manufacturing – Advanced Research in Virtual and Rapid Prototyping (eds. P. Bartolo et al.), Taylor & Francis, 2010. (doi: 10.1201/9780203859476.ch36)

(19) Gomes, C.M., Rambo, C.R., Oliveira, A.P.N., Hotza, D., Gouvea, D., Travitzky, N., Greil, P., Colloidal processing of glass ceramics for Laminated Object Manufacturing, Journal of the American Ceramic Society, 92, 1186 – 1192, 2009

(20) C. Wanpeng, L.L. Hench " Bioactive materials", 1996,pages 493-507

(21)Chengtie Wu, Jiang Chang “A review of bioactive silicate ceramics”
(22)Yasumasa Akagawa, Masaki Hashimoto,Noriaki Kondo, Kelichi Satomi, Hiromichi Tsuru,”Initial bone-implant interfaces of submergible and supramergible endosseous single-crystal sapphire implants”,1986,pages 96-100
(23)M.A.Malik,D.A.Puleo,R.Bizios,R.H. Doremus,”Osteoblasts on hydroxyapatite, alumina and bone surfaces *in vitro*;morphology during the first 2 h of attachment”,1992.
(24)L.L.Hench,”The story of Bioglass”,2006
(25)Q.Z.Chen,I.D.thompson,A.R.Boccaccini,”45S5 Bioglass derived glass-ceramic scaffolds for bone tissue engineering”,2005
(26)N.Ignjatovic, S.Tomic,M. Dakic, M.Miljkovic, M.Plavsic, D.Uskokovic, “Synthesis and properties of hydroxyapatite/poly-L-lactide composite biomaterials”,1999
(27)L.L.Hench, H.A. Paschall,” Direct chemical bond of bioactive glass-ceramic materials to bone and muscle”,2005
(28)Vassilis Karageorgiou , David Kaplan “Porosity of 3d biomaterials scaffolds and osteogenesis”
(29)S.M. Best,A.E.Porter , E.S.Thian ,J.Huan: “Bioceramics: past, present and for future”.*J.Eur Ceram Soc* 2008;28:1319-27.
(30)S.V.Dorozhkin, “Bioceramics of calcium orthophosphates”, *Biomaterials*,2010,31:1465-85;
(31)X.liu, M.Morra, A.Carpi, B.Li, ”Bioactive calcium silicate ceramics and coatings”,2008
(32)T.Kokubo,”Bioactive glass ceramics: properties and applications”,1991
(33)P. Torricelli, M.Fini, G.Giavaresi, M.Rocca, G.Pierini, R.Giardino “Isolation and characterization of osteoblast cultures from normal and osteopenic sheep for biomaterials evaluation” ,2000
(34)L.L. Hench, J.Wilson,” An introduction to bioceramics”,Word Scientific Publishing,1993
(35)Maddalena Mastrogiacomo, Silvia Scaglione, Roberta Martinetti, Laura Dolcini, Francesco Beltrame, Ranieri Cancedda, Rodolfo Quaro “Role of scaffold internal structure on in vivo bone formation in macro porous calcium phosphate bioceramics”
(36)A.Krajewski, A. Ravaglioli, A. Tinti, P. Taddei, M.Mazzocchi, R.Martinetti, C.Fagnano, M.Fini ”Comparison between the *in vitro* surface transformations of AP40and RKKP bioactive glasses”,2005
(37)Paolo Colombo, Gabriela Mera, Ralf Riedel, Gian Domenico Sorarù “Polymer-derived ceramics:40 years of research and innovation in advanced ceramics”
(38)R. Riedel,G. Mera,R. Hauser,A. Klonczynski,” Silicon-Based Polymer-derived Ceramics: Synthesis Properties and Applications-A. Review”,2006,pag.425-444
(39)E. Bernardo,P. Colombo, I. Caciotti,A. Bianco, R. Bedini, R. Pecci, K. Pardun, L. Treccani, K. Rezwan,” Porous wollastonite-hydroxyapatite bioceramics from a preceramic polymer and micro- or nano- sized fillers” ,2011.
(40)P.Greil, “Active-Filler-Controlled Pyrolysis of Preceramic Polymers”,1995
(41)E. Bernardo, E. Tomasella, P. Colombo, “ development of multiphase bioceramics from a filler containing preceramic polymer”; Ceramics International 35 (2009) 1415-1421
(42)Xiaoke Li, Jiang Chang, “ Preparation and Characterization of bioactive collagen/wollastonite composite scaffolds”,2005.
(43)Tadashi Kokubo,“Bioactive glass ceramics: properties and application”

(44)Masahiko Kobayashi, Dr. Takashi Nakamura, Yoshifumi Okada, Akira Fukumoto, Taizo Furukawa, Hirofumi Kato, Tadashi Kokubo, Takemi Kikutani, " bioactive bone cement:comparison of apatite and wollastonite containing glass-ceramic, hydroxyapatite, and β-tricalcium phosphate fillers on bone-bonding strength",1998.
(45)M.Neo, T. Nakamura, C.Ohtsuki, T.Kokubo, T. Yamamuro," Apatite formation on three kinds of bioactive material at an early stage *in vivo*: a comparative study by transmission electron microscopy",2004.
(46)I.Asahina et al.,J.Med.Dent.Sci.44, 63 (1997)
(47)A.Guo, J.K.Beddow, A.F.Vetter," A simple relationship between particle shape effects and density, flow rate and Hausner Ratio"
(48)A.Martin,Ph.D. Thomas,"Tablets & Capsules,Powder Density in Solid Dosage Forms".
(49)E.C.Abdullah, D. Geldart," the use of bulk density measurements as flowability indicators",1998.
(50)Andreas Borger, Peter Supancic, Robert Danzer, " The ball on three balls test for strength testing of brittle discs: stress distribution in the disc",2001
(51)Robert Danzer, Walter Harrer, Peter Supancic, Tanja Lube, Zhonghua Wang, Andreas Borger "The ball on three balls test – strength and failure analysis of different materials",2006
(52)Andreas Borger, Peter Supancic, Robert Danzer, "the ball on three balls test for strength testing of brittle discs; Part II: analysis of possible errors in the strength determination",2003
(53)M.Arnold,A.R.Boccaccini, G.Ondracek,"Prediction of Poisson's ratio of porous material",1996
(54)T.Kokubo,S.Ito,M. Shigematsu,S.Sakka,"Mechanical properties of a new type of apatite-containing glass-ceramic for prosthetic application",1985.
(55)M.Guglielmi,Dispense per il corso di Materiali Ceramici,2008-2009.

Acknowledgements

My gratitude goes to Professor Jens Günster and to Dr. Gomes Cynthia M. for the chance that they gave me to study at BAM in Berlin.
Many thanks also to all friendly and wonderful people that I have met at BAM, it was a pleasure to work with them.

Ringrazio il Professor Paolo Colombo per avermi dato la possibilità di vivere questa esperienza e per avermi supportato in questi mesi. Ringrazio inoltre il Professor Enrico Bernardo per i consigli che ha dato durante il periodo di ricerca.
Un grosso ringraziamento va inoltre ad Andrea Zocca per avermi supportato in questi mesi di ricerca al BAM e per il suo aiuto nella scrittura della tesi, senza di lui tutto ciò sarebbe stato molto più difficile.

Ringrazio inoltre i miei genitori e i miei fratelli, senza di loro tutto ciò sarebbe stato impossibile, dedico a loro questo lavoro!
Infine grazie a tutti i miei amici che mi hanno aiutato in questo percorso di studi!